J. Fluid Mech. (1993), *vol.* 254, *pp.* 671–699

On the dynamics of buoyant and heavy particles in a periodic Stuart vortex flow

By KEK-KIONG TIO[1], AMABLE LIÑÁN[2],
JUAN C. LASHERAS[1]
AND ALFONSO M. GAÑÁN-CALVO[3]

[1]Department of Applied Mechanics and Engineering Sciences, University of California,
La Jolla, CA 92093-0411, USA

[2]E.T.S. Ingenieros Aeronauticos, Plaza del Cardenal Cisneros 3, Universidad Politécnica de
Madrid, 28040 Madrid, Spain

[3]Departamento de Ingeniería Energética y Fluidomecánica, E.T.S. Ingenieros Industriales,
Universidad de Sevilla, 41012 Sevilla, Spain

(Received 31 July 1992 and in revised form 19 March 1993)

In this paper, we study the dynamics of small, spherical, rigid particles in a spatially periodic array of Stuart vortices given by a steady-state solution to the two-dimensional incompressible Euler equation. In the limiting case of dominant viscous drag forces, the motion of the particles is studied analytically by using a perturbation scheme. This approach consists of the analysis of the leading-order term in the expansion of the 'particle path function' Φ, which is equal to the stream function evaluated at the instantaneous particle position. It is shown that heavy particles which remain suspended against gravity all move in a periodic asymptotic trajectory located above the vortices, while buoyant particles may be trapped by the stable equilibrium points located within the vortices. In addition, a linear map for Φ is derived to describe the short-term evolution of particles moving near the boundary of a vortex. Next, the assumption of dominant viscous drag forces is relaxed, and linear stability analyses are carried out to investigate the equilibrium points of the five-parameter dynamical system governing the motion of the particles. The five parameters are the free-stream Reynolds number, the Stokes number, the fluid-to-particle mass density ratio, the distribution of vorticity in the flow, and a gravitational parameter. For heavy particles, the equilibrium points, when they exist, are found to be unstable. In the case of buoyant particles, a pair of stable and unstable equilibrium points exist simultaneously, and undergo a saddle-node bifurcation when a certain parameter of the dynamical system is varied. Finally, a computational study is also carried out by integrating the dynamical system numerically. It is found that the analytical and computational results are in agreement, provided the viscous drag forces are large. The computational study covers a more general regime in which the viscous drag forces are not necessarily dominant, and the effects of the various parametric inputs on the dynamics of buoyant particles are investigated.

1. Introduction

The motion of bubbles, drops, and solid particles in fluid flows is a widely encountered phenomenon and has important implications in many technological applications.

In many instances, the fluid medium carrying the particles (i.e. bubbles, drops, or solid particles) is in a state of motion involving large-scale vortical structures, and the purpose of this paper is to elucidate the dynamics of particles in a class of spatially periodic vortical flows. Specifically, we will study the motion of small, spherical, rigid particles in a periodic array of vortices given by Stuart's (1967) solution to the two-dimensional, steady-state, incompressible Euler equation. In this paper, we assume that the size of the particles and their concentration are sufficiently small so that their mutual interactions as well as their effects on the base flow can be neglected.

The motion of a small spherical particle in an unsteady, non-uniform flow field $\boldsymbol{u}$ is governed by the momentum equation (see Maxey & Riley 1983; Auton, Hunt & Prud'homme 1988)

$$\frac{\pi}{6}d^3\left(\rho_P+0.5\rho_F\right)\frac{\mathrm{d}\boldsymbol{V}}{\mathrm{d}t}=\frac{\pi}{6}d^3\left(\rho_P-\rho_F\right)\boldsymbol{g}+\frac{\pi}{4}d^3\rho_F\frac{\mathrm{D}\boldsymbol{u}}{\mathrm{D}t}+\boldsymbol{F}_d+\boldsymbol{F}_l+\boldsymbol{F}_h \tag{1.1}$$

together with

$$\frac{\mathrm{d}\boldsymbol{x}_P}{\mathrm{d}t}=\boldsymbol{V}, \tag{1.2}$$

where $\boldsymbol{x}_P$ and $\boldsymbol{V}$ are the particle's position and velocity, respectively. In (1.1), d is the particle diameter, ρ is the density, $\boldsymbol{g}$ is the gravitational acceleration, and the subscripts F and P refer to the fluid and particle, respectively. The five terms on the right-hand side are the forces on the particle contributed by gravity, the acceleration of the fluid particle, viscous drag, lift, and the Basset history. The coefficient of 0.5 in the left-hand side accounts for the effects of the added mass on an accelerating sphere. The three forces, $\boldsymbol{F}_d$, $\boldsymbol{F}_l$, and $\boldsymbol{F}_h$ are functions of the velocity of the particle relative to the fluid velocity. The viscous drag takes the form of

$$\boldsymbol{F}_d=3\pi d\nu\rho_F f_d\left(\boldsymbol{u}-\boldsymbol{V}\right), \tag{1.3}$$

where ν is the fluid kinematic viscosity, and f_d is a coefficient correcting for the effects of non-zero Reynolds number $Re_P=|\boldsymbol{u}-\boldsymbol{V}|\,d/\nu$. Based on the study of Saffman (1965), which is valid for $Re_P << 1$ (Stokes regime), and the work of Auton *et al.* (1988), which is applicable to inviscid flows ($Re_P \rightarrow \infty$), we can write the lift force as

$$\boldsymbol{F}_l=\begin{cases}1.615\rho_F\nu^{\frac{1}{2}}d^2\,|\phi|^{\frac{1}{2}}\,\mathrm{sign}\,(\phi)\,\boldsymbol{n}, & Re_P<<1\\[2ex] \dfrac{\pi}{12}d^3\rho_F\left(\boldsymbol{u}-\boldsymbol{V}\right)\times\boldsymbol{\omega}, & Re_P>>1.\end{cases} \tag{1.4}$$

In (1.4), $\boldsymbol{\omega}$ is the vorticity of the flow field. We note that the lift force for $Re_P << 1$ given above is valid only for two-dimensional flows in the (x,y)-plane with

$$\phi=\left(u_x-V_x\right)^2\frac{\partial u_x}{\partial y}-\left(u_y-V_y\right)^2\frac{\partial u_y}{\partial x}-\left(u_x-V_x\right)\left(u_y-V_y\right)\left(\frac{\partial u_x}{\partial x}-\frac{\partial u_y}{\partial y}\right) \tag{1.5}$$

and

$$\boldsymbol{n}=\frac{1}{|\boldsymbol{u}-\boldsymbol{V}|}\left[-\left(u_y-V_y\right)\boldsymbol{e}_x+\left(u_x-V_x\right)\boldsymbol{e}_y\right]. \tag{1.6}$$

In (1.6), $\boldsymbol{e}_x$ and $\boldsymbol{e}_y$ are unit vectors in the x- and y-directions, respectively. According to a recent work of McLaughlin (1991), the original formula of Saffman (1965) and, therefore, its counterpart in (1.4) overpredict the actual lift force. Mei (1992) has recently obtained a correlation for the lift force for $Re_P < 100$, using the result of Saffman (1965) and the numerical findings of Dandy & Dwyer (1990). The discrepancy between Mei's (1992) correlation and the formula of Auton *et al.* (1988), which is valid only for the case of $Re_P \rightarrow \infty$, is less than 25% at $Re_P = 100$. The Basset history force is given by Maxey & Riley (1983) for the Stokes regime ($Re_P \rightarrow 0$) as

$$\boldsymbol{F}_h = \tfrac{3}{2} d^2 \rho_F (\pi \nu)^{\frac{1}{2}} \int_0^t \frac{1}{(t-\sigma)^{\frac{1}{2}}} \left(\frac{\mathrm{d}\boldsymbol{u}}{\mathrm{d}\sigma} - \frac{\mathrm{d}\boldsymbol{V}}{\mathrm{d}\sigma} \right) \mathrm{d}\sigma. \qquad (1.7)$$

We note here that the validity of (1.7) has recently been brought into question by the works of Reeks & McKee (1984) and Mei, Lawrence & Adrian (1991). It is pointed out by Mei *et al.* (1991) that (1.7) is applicable only in the Stokes regime, in which it is not even uniformly valid over the time domain; the kernel in (1.7) behaves like $(t-\sigma)^{-\frac{1}{2}}$ only for short time, but decays much faster for long time. For simplicity, the lift force and the history term will be neglected in this paper. Thus, unless stated otherwise, we include only the effects of particle inertia, added mass, gravity, fluid acceleration, and the viscous drag in the momentum equation.

Equation (1.1), or its simplified version, has been applied to numerous studies of particles in non-uniform fluid flows. Chein & Chung (1987, 1988) retain only the viscous drag term in their studies of heavy particles in plane free shear layers. In the first paper, emphasis is placed on the effects of 'vortex pairing' on the dynamics of the particles, while the second paper covers a wider range of the vortex street. The same simplified version of (1.1) is also employed by Chung & Troutt (1988) in their study of heavy particles in an axisymmetric jet. The numerical results of these studies essentially show the same phenomenon: for particles with a small Stokes number (or, equivalently, a small diameter), their lateral dispersion by the vortices increases with increasing Stokes number (or diameter) until a maximum is reached, after which the dispersion tappers off as the Stokes number is increased. This trend of dispersion versus the Stokes number has also been observed in an earlier study by Crowe, Gore & Troutt (1985). In their study, the two-dimensional free shear layer is modelled with a row of Stuart vortices; again, they retain the viscous drag force only.

A more detailed study of the motion of heavy particles in the Stuart vortex flow is presented in a paper by Gañán-Calvo & Lasheras (1991), who retain the viscous drag force and the gravity term in the momentum equation. They find that depending on the initial conditions, particles may either settle due to the pull of gravity or remain indefinitely suspended in open trajectories above the vortices. When suspension occurs, the particles either move in periodic, quasi-periodic, or chaotic trajectories. In the chaotic regime, suspended particles become 'fluidized' in a layer of finite thickness located above the vortices. Furthermore, for suspended particles with a small diameter, they all asymptotically collect along a single periodic trajectory. However, as the diameter increases, this periodic trajectory bifurcates into two quasi-periodic orbits, which in turn evolve in a cascade of bifurcations resulting in chaotic trajectories; beyond a certain critical diameter, no particle can be suspended. In some sense, then, this finding of Gañán-Calvo & Lasheras (1991) is qualitatively similar to the relation between particle dispersion and the Stokes number observed by Crowe *et al.* (1985), Chein & Chung (1987, 1988), and Chung & Troutt (1988). In a recent study (Tio, Gañán-Calvo & Lasheras 1993*a*), the work of Gañán-Calvo & Lasheras (1991) is extended to include in (1.1) the forces contributed by the fluid acceleration and the lift of Auton *et al.* (1988). A consequence of the inclusion of the fluid-acceleration term, in addition to the gravitational and viscous drag forces, is to greatly enrich the dynamics of the particles. Not only can they be suspended above the vortices, but particles denser than the fluid can also be suspended below the vortices or be suspended intermittently above and below the vortices; in addition, closed particle orbits are also observed. While only a relatively small portion of the result of Tio *et al.* (1993*a*) is obtained by taking into account the lift force in (1.1), a conjecture can nevertheless be made that its inclusion does not qualitatively alter the topography of open-trajectory suspensions.

In the case of buoyant particles in the Stuart vortex flow, we do not find any suspension of particles in open trajectories above or below the vortices. Nor can we find any closed particle trajectory. As will be seen later, a buoyant particle or a bubble, for that matter, either escapes (due to its buoyancy), or is captured by a vortex and remains trapped at the equilibrium point near the centre of that vortex.

The entrapment of bubbles or other buoyant particles by a vortex has also been observed in other types of vortical flows. Maxey (1987), in a numerical study of particles as well as bubbles in a Langmuir cellular flow field, finds that all the bubbles released in the flow are trapped by the equilibrium points in the flow field if the bubble rise speed in still fluid, Q, is sufficiently small. As Q is increased, some of the bubbles escape from captivity, rising through the upflow regions of the flow field. When Q is increased beyond a critical value, the equilibrium points no longer exist, and all the bubbles accumulate and rise along asymptotic paths. The equation used by Maxey (1987), however, is based on the assumption of a Stokes-flow regime, and is slightly different from (1.1). The entrapment of buoyant particles by a stable equilibrium point has also been observed numerically by Crisanti *et al.* (1990). In their study, the selected flow field is similar to the Langmuir cellular flow studied by Maxey (1987). In a numerical simulation of the trajectories of bubbles released below a line vortex with a horizontal axis, Thomas *et al.* (1983, 1984) find that all bubbles passing the vortex within a critical distance from the centre are trapped by the vortex. Furthermore, this critical distance increases with the strength of the vortex. In an asymptotic analysis carried out by Nielsen (1984), it is shown that buoyant particles may be trapped by a stable equilibrium point of the flow field generated by a vortex of solid-body rotation.

In this paper, we first develop an approximate analytical technique to study the dynamics of particles in a Stuart vortex flow. This approximate analysis, which is based on the assumption that viscous drag is the dominant force acting on a particle, is valid for bubbles, drops, and solid particles. Furthermore, it reveals that there are, generally speaking, two mechanisms by which particles are suspended against gravity in the mixing region of the flow. The first mechanism, by which particles heavier than the fluid are suspended in motion along open trajectories above the vortices, has been observed in the numerical studies of Gañán-Calvo & Lasheras (1991) and Tio *et al.* (1993*a*). For buoyant particles, however, the suspension mechanism is completely different from that of heavy particles. Owing to the existence of a stable equilibrium point inside each vortex for buoyant particles, the suspension mechanism consists of particle entrapment by the vortices so that a buoyant particle which does not escape from a vortex is captured by the equilibrium point located inside the vortex. To test the validity of the prediction of the approximate analytical model that buoyant and heavy particles are suspended in the flow by two different mechanisms, we next study the linear stability of the fixed points of the dynamical system governing the motion of the particles. Here, we relax the assumption of dominant viscous drag, and find that the results are consistent with the asymptotic model. Finally, we carry out a computational study by integrating numerically the dynamical system, and compare the results with the asymptotic model to ascertain its accuracy.

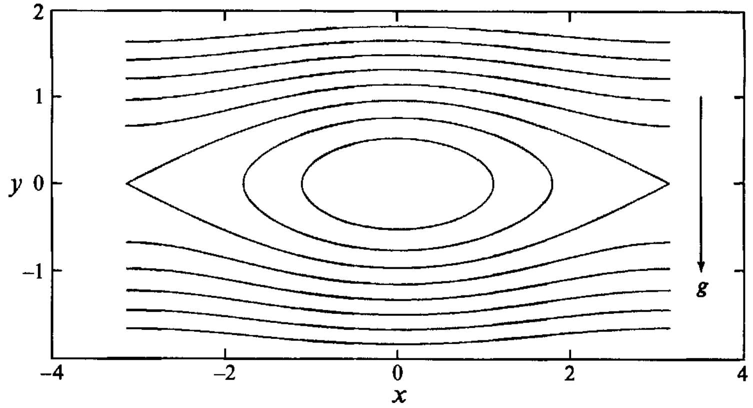

FIGURE 1. A Stuart vortex and streamlines for $k = 0.25$. Note that gravity points in the negative y-direction, and that x and y are dimensionless.

2. Problem formulation

The flow field selected for our study consists of a periodic array of Stuart vortices (Stuart 1967). The stream function Ψ associated with the flow is given by

$$\Psi = \frac{\lambda U_\infty}{2\pi} \ln \left[\cosh\left(\frac{2\pi y}{\lambda}\right) - k\cos\left(\frac{2\pi x}{\lambda}\right)\right], \tag{2.1}$$

which satisfies the inviscid vorticity equation $\nabla^2\Psi = \omega(\Psi)$. The vorticity takes the form of

$$\omega(\Psi) = \frac{2\pi U_\infty}{\lambda}\left(1-k^2\right) \mathrm{e}^{-4\pi\Psi/\lambda U_\infty}. \tag{2.2}$$

In (2.1) and (2.2), U_∞ is the free-stream velocity, λ is the distance between two contiguous vortices, and k is a parameter which determines the distribution of vorticity. For $k = 0$ (2.1) reduces to a $\tanh y$ shear layer, while $k = 1$ corresponds to a row of point vortices. In figure 1, we show one of the vortices together with the streamlines. In this paper, the terms 'cat's eye' and 'Stuart vortex' are used interchangeably. The fluid velocity $\boldsymbol{u} = \left(u_x, u_y\right)$ is given by

$$u_x = -\frac{\partial \Psi}{\partial y} = -\frac{\sinh\left(2\pi y/\lambda\right)}{\cosh\left(2\pi y/\lambda\right) - k\cos\left(2\pi x/\lambda\right)} U_\infty, \tag{2.3}$$

$$u_y = \frac{\partial \Psi}{\partial x} = \frac{k\sin\left(2\pi x/\lambda\right)}{\cosh\left(2\pi y/\lambda\right) - k\cos\left(2\pi x/\lambda\right)} U_\infty. \tag{2.4}$$

Introducing the dimensionless quantities

$$x^* = \frac{x}{\lambda/2\pi}, \tag{2.5}$$

$$\boldsymbol{u}^* = \frac{\boldsymbol{u}}{U_\infty}, \quad \boldsymbol{V}^* = \frac{\boldsymbol{V}}{U_\infty}, \tag{2.6}$$

$$t^* = \frac{t}{\lambda/2\pi U_\infty}, \tag{2.7}$$

$$\varepsilon = \frac{\rho_F}{\rho_P + 0.5\rho_F}, \tag{2.8}$$

$$g^* = \frac{\boldsymbol{g}}{g}, \tag{2.9}$$

we obtain the dimensionless counterpart of (1.1) and (1.2), the lift and history forces being excluded, as

$$\frac{\mathrm{d}x_P^*}{\mathrm{d}t^*} = V_x^*, \tag{2.10}$$

$$\frac{\mathrm{d}y_P^*}{\mathrm{d}t^*} = V_y^*, \tag{2.11}$$

$$\frac{\mathrm{d}V_x^*}{\mathrm{d}t^*} = \tfrac{3}{2}\varepsilon \boldsymbol{u}^* \cdot \nabla u_x^* + \left(u_x^* - V_x^*\right) A f_d, \tag{2.12}$$

$$\frac{\mathrm{d}V_y^*}{\mathrm{d}t^*} = \tfrac{3}{2}\varepsilon \boldsymbol{u}^* \cdot \nabla u_y^* + \left(u_y^* - V_y^*\right) A f_d + \left(\tfrac{3}{2}\varepsilon - 1\right) B, \tag{2.13}$$

where

$$A \equiv \frac{18\varepsilon\nu\lambda}{2\pi U_\infty d^2}, \tag{2.14}$$

$$B \equiv \frac{\lambda g}{2\pi U_\infty^2}. \tag{2.15}$$

The parameter A as defined in (2.14) is the inverse of the Stokes number, which is equal to the ratio of the particle relaxation time $(d^2/18\varepsilon\nu)$ to the fluid residence time $(\lambda/2\pi U_\infty)$, and is a measure of how under the effect of viscosity a particle responds to a given fluctuation in the flow field. The parameter B is a measure of the relative strength of gravitational effects, and is similar to the inverse of the Froude number. It should be noted from (2.13) that we have chosen gravity to point in the direction opposite to the y-axis. The density ratio has the range of $0 \leqslant \varepsilon \leqslant 2$; for heavy particles $\varepsilon < 2/3$, for buoyant particles $\varepsilon > 2/3$, and $\varepsilon = 2$ for bubbles. The drag coefficient f_d can be calculated by making use of the correlations given by Clift, Grace & Weber (1978) for rigid particles. In the case of bubbles, Oliver & Chung (1987) have recently proposed a correlation valid for the Stokes regime and beyond. These correlations are given in terms of the Reynolds number of the particle based on the relative velocity between the particle and the fluid:

$$Re_P \equiv \frac{|\boldsymbol{u} - \boldsymbol{V}|\, d}{\nu}. \tag{2.16}$$

This instantaneous particle Reynolds number is related to the free-stream Reynolds number, $Re \equiv U_\infty d/\nu$, through the formula

$$Re_P = |\boldsymbol{u}^* - \boldsymbol{V}^*|\, Re. \tag{2.17}$$

In our computer program, we assume the particles to be rigid, and include all the correlations given by Clift *et al.* (1978) for f_d valid over different ranges of Re_P. However, all the numerical results presented in this paper correspond to the range of $0 < Re_P < 200$, in which case the single correlation of

$$f_d = 1 + 0.1315 Re_P^{0.82 - 0.05 \log_{10} Re_P} \tag{2.18}$$

is applicable with an error of less than 2%. In (2.18), the first term on the right-hand side corresponds to the Stokes drag while the second term accounts for the correction of non-zero Re_P. The dimensionless fluid velocity $\boldsymbol{u}^* = \left(u_x^*, u_y^*\right)$ and vorticity ω^* are given by

$$u_x^* = -\frac{\sinh y^*}{\cosh y^* - k\cos x^*}, \tag{2.19}$$

$$u_y^* = \frac{k\sin x^*}{\cosh y^* - k\cos x^*}, \tag{2.20}$$

$$\omega^* = \frac{1-k^2}{[\cosh y^* - k\cos x^*]^2}. \tag{2.21}$$

It should be observed from the system of equations (2.10)–(2.13) that the dynamics of particles is governed by a set of five parameters: the vorticity-distribution parameter k, the free-stream Reynolds number Re, the parameter A, the gravitational parameter B, and the density ratio ε. For convenience, we will drop the asterisks from now on. Unless stated otherwise, we will deal with dimensionless quantities only.

3. Analysis of dominant viscous drag

For small solid particles, drops, or bubbles moving in a liquid medium, $\varepsilon \sim O(1)$ and $(d/\lambda) << 1$. Thus, with a moderate free-stream Reynolds number Re, the parameter A is usually a large number, and the viscous drag is the dominant force acting on the particles. As a result, the velocity of the particles is almost equal to that of the fluid and, due to a moderate Re, the Reynolds number Re_P becomes much smaller than unity. In what follows, we assume that $f_d = 1$ (Stokes drag) and that the product $C = Af_d$ is a constant much greater than unity, and under this condition we analyse the evolution of the dynamics of the particles.

In this special case of $\gamma \equiv 1/C \ll 1$, we see that the system of (2.10)–(2.13) together with the initial conditions

$$x_P(t=0) = x_{P0}, \qquad y_P(t=0) = y_{P0}, \tag{3.1}$$

$$V_x(t=0) = V_{x0}, \qquad V_y(t=0) = V_{y0}, \tag{3.2}$$

constitute a singularly perturbed initial value problem, γ being the small parameter. In the 'outer region' of the time domain, (2.10)–(2.13) reduce to the system of

$$\frac{\mathrm{d}x_P}{\mathrm{d}t} = V_x, \tag{3.3}$$

$$\frac{\mathrm{d}y_P}{\mathrm{d}t} = V_y, \tag{3.4}$$

$$V_x = u_x + \gamma\left[-\frac{\mathrm{d}V_x}{\mathrm{d}t} + \tfrac{3}{2}\varepsilon\boldsymbol{u}\cdot\nabla u_x\right], \tag{3.5}$$

$$V_y = u_y + \gamma\left[-\frac{\mathrm{d}V_y}{\mathrm{d}t} + \tfrac{3}{2}\varepsilon\boldsymbol{u}\cdot\nabla u_y + \left(\tfrac{3}{2}\varepsilon - 1\right)B\right], \tag{3.6}$$

which consists of two ordinary differential equations and two algebraic equations so that the initial conditions given by (3.1) and (3.2) cannot, in general, be satisfied completely. In the 'inner region' characterized by $t \sim O(\gamma)$, we introduce the timescale $\tilde{t}$ given by

$$\tilde{t} = \frac{t}{\gamma} \sim O(1), \tag{3.7}$$

and rescale (2.10)–(2.13) to obtain

$$\frac{\mathrm{d}x_P}{\mathrm{d}\tilde{t}} = \gamma V_x, \tag{3.8}$$

$$\frac{\mathrm{d}y_P}{\mathrm{d}\tilde{t}} = \gamma V_y, \tag{3.9}$$

$$\frac{\mathrm{d}V_x}{\mathrm{d}\tilde{t}} = (u_x - V_x) + \gamma\left[\tfrac{3}{2}\varepsilon \boldsymbol{u}\cdot\nabla u_x\right], \tag{3.10}$$

$$\frac{\mathrm{d}V_y}{\mathrm{d}\tilde{t}} = \left(u_y - V_y\right) + \gamma\left[\tfrac{3}{2}\varepsilon \boldsymbol{u}\cdot\nabla u_y + \left(\tfrac{3}{2}\varepsilon - 1\right)B\right]. \tag{3.11}$$

Then, the complete solution of the original initial value problem consists of integrating (3.8)–(3.11) subject to the initial conditions given by (3.1) and (3.2), integrating (3.3) and (3.4), and carrying out an asymptotic matching in the time domain where the 'inner' and 'outer' solutions overlap. This asymptotic matching is needed to calculate the constants in the integrals of (3.3) and (3.4). In this paper, we are interested in the 'outer region' only. However, before we begin our analysis, we shall present a brief discussion on the 'inner region'.

In the 'inner region', the leading-order approximation to the solution of (3.8)–(3.11) and (3.1)–(3.2) can be easily obtained as

$$x_P = x_{P0} + O(\gamma), \tag{3.12}$$

$$y_P = y_{P0} + O(\gamma), \tag{3.13}$$

$$V_x = u_{x0} - (u_{x0} - V_{x0})\,\mathrm{e}^{-\tilde{t}} + O(\gamma), \tag{3.14}$$

$$V_y = u_{y0} - \left(u_{y0} - V_{y0}\right)\mathrm{e}^{-\tilde{t}} + O(\gamma), \tag{3.15}$$

where $\left(u_{x0}, u_{y0}\right)$ is the fluid velocity evaluated at the initial particle position (x_{P0}, y_{P0}). Thus, the position of the particle changes very slowly, but its velocity experiences a rapid change with time $\tilde{t}$ and exponentially approaches $\left(u_{x0}, u_{y0}\right)$.

Beyond the 'inner region', the viscous drag acting on a particle has forced it to move with the local fluid velocity, except for a small deviation of order γ [see (3.5) and (3.6)]. In other words, the trajectory of the particle is almost a streamline characterized by a constant value of Ψ. Owing to the perturbative terms of $O(\gamma)$ in (3.5) and (3.6), which will be examined in detail later, the particle cannot move exactly along a streamline. Instead, it slowly drifts away from it. To examine the drift of the particle, we first introduce the 'particle path function' Φ, which is defined by

$$\Phi \equiv \Psi\left(x_P(t), y_P(t)\right). \tag{3.16}$$

That is, the 'particle path function' is simply the stream function evaluated at the instantaneous position of the particle along its trajectory. Since the particle drifts slowly from a streamline, Φ changes only by a small amount of order γ during a time period of $\Delta t \sim O(1)$ but its change will be significant in a time interval of order $1/\gamma$. Thus, the dynamics of the particle actually constitute a multiple-scale problem involving the fast time t and the slow-time variable $\tau = \gamma t$. In this paper, we are interested in the short-term evolution of the particle and, thus, deal with the fast variable t only. From (3.16), we obtain the rate of change of Φ as

$$\frac{\mathrm{d}\Phi}{\mathrm{d}t} = \left.\frac{\partial\Psi}{\partial x}\right|_P \frac{\mathrm{d}x_P}{\mathrm{d}t} + \left.\frac{\partial\Psi}{\partial y}\right|_P \frac{\mathrm{d}y_P}{\mathrm{d}t} = u_y V_x - u_x V_y, \tag{3.17}$$

where the fluid velocity, $\boldsymbol{u}$, is evaluated at the instantaneous position of the particle. The velocity of the particle can be expanded asymptotically as

$$\boldsymbol{V} = \boldsymbol{u}(\boldsymbol{x}_P) + \gamma \boldsymbol{V}^{(1)}(t, \boldsymbol{x}_P) + O\left(\gamma^2\right), \tag{3.18}$$

where $\boldsymbol{V}^{(1)} = \left(V_x^{(1)}, V_y^{(1)}\right)$ are unknowns to be determined. Substituting (3.18) and its derivative,

$$\frac{\mathrm{d}\boldsymbol{V}}{\mathrm{d}t} = \boldsymbol{u} \cdot \nabla \boldsymbol{u} + \gamma \left(\boldsymbol{u} \cdot \nabla \boldsymbol{V}^{(1)} + \boldsymbol{V}^{(1)} \cdot \nabla \boldsymbol{u} + \frac{\partial \boldsymbol{V}^{(1)}}{\partial t} \right) + O\left(\gamma^2\right), \tag{3.19}$$

into the system of (2.12)–(2.13), we then obtain

$$\boldsymbol{V}^{(1)} = \left(\tfrac{3}{2}\varepsilon - 1\right) \left[\boldsymbol{u} \cdot \nabla \boldsymbol{u} + B\boldsymbol{e}_y\right]. \tag{3.20}$$

Had the Basset history and the Saffman lift force been included in (2.12)–(2.13), their effects would first appear at $O(\gamma^{\frac{3}{2}})$. That is, the right-hand side of (3.18) would consist of an additional term of the form $\gamma^{\frac{3}{2}} \boldsymbol{V}^{(\frac{3}{2})}$, where

$$\boldsymbol{V}^{(\frac{3}{2})} = \frac{2.284}{\pi} \varepsilon^{\frac{1}{2}} \operatorname{sign}(\phi) K \left(V_y^{(1)} \boldsymbol{e}_x - V_x^{(1)} \boldsymbol{e}_y\right) - \frac{3}{(2\pi)^{\frac{1}{2}}} \varepsilon^{\frac{1}{2}} \int_0^t \frac{\boldsymbol{u} \cdot \nabla \boldsymbol{V}^{(1)}}{(t-\sigma)^{\frac{1}{2}}} \, \mathrm{d}\sigma. \tag{3.21}$$

The quantity K in (3.21) is given by

$$K = \frac{\left| V_x^{(1)} \left(V_x^{(1)} \dfrac{\partial u_x}{\partial y} - V_y^{(1)} \dfrac{\partial u_x}{\partial x} \right) + V_y^{(1)} \left(V_x^{(1)} \dfrac{\partial u_y}{\partial y} - V_y^{(1)} \dfrac{\partial u_y}{\partial x} \right) \right|^{\frac{1}{2}}}{\left(\left\{V_x^{(1)}\right\}^2 + \left\{V_y^{(1)}\right\}^2 \right)^{\frac{1}{2}}}. \tag{3.22}$$

Thus, in the special case of dominant viscous drag, the lift and history forces can be neglected in comparison with the others acting on the particle. With the velocity of the particle given by the expansion

$$\boldsymbol{V} = \boldsymbol{u} + \gamma \left(\tfrac{3}{2}\varepsilon - 1\right) \left[\boldsymbol{u} \cdot \nabla \boldsymbol{u} + B\boldsymbol{e}_y\right] + O\left(\gamma^2\right), \tag{3.23}$$

we then obtain from (3.17) the rate of change of Φ as

$$\frac{\mathrm{d}\Phi}{\mathrm{d}t} = \left[(\boldsymbol{u} \cdot \nabla u_x) u_y - (\boldsymbol{u} \cdot \nabla u_y) u_x - B u_x\right] \left(\tfrac{3}{2}\varepsilon - 1\right) \gamma + O\left(\gamma^2\right). \tag{3.24}$$

To further investigate the motion of the particle, an integration of (3.24) is required. Before we do that, however, we present here some comments pertaining to (3.23). Basically, it states that, after the initial transient, the velocity of the particle is equal to the local fluid velocity, except for a small perturbation which results from the density difference between the particle and the fluid. The first term in the order-γ perturbation is due to the fact that a particle with a different mass density (inertia) cannot accelerate as much as the fluid; the second term is due to gravity, the quantity $\gamma\left(\frac{3}{2}\varepsilon - 1\right) B$ being the terminal rising/settling speed of the particle in quiescent fluid. An expression similar to (3.23) has been proposed by Stommel (1949), who ignores the effect of particle inertia and the advective acceleration of the fluid. In this case, the velocity of the particle can be written as

$$\boldsymbol{V} = -\frac{\partial \Psi_P}{\partial y} \boldsymbol{e}_x + \frac{\partial \Psi_P}{\partial x} \boldsymbol{e}_y = \boldsymbol{u} + \left(\tfrac{3}{2}\varepsilon - 1\right) \frac{B}{A} \boldsymbol{e}_y, \tag{3.25}$$

where Ψ_P is the 'particle stream function' given by

$$\Psi_P(x, y) = \Psi(x, y) + \left(\tfrac{3}{2}\varepsilon - 1\right) \frac{B}{A} x. \tag{3.26}$$

Particle trajectories are then represented by the contours of Ψ_P. For the Langmuir cellular flow considered by Stommel (1949), which is composed of spatially periodic convection rolls, these contours consist of open and closed curves. Thus, heavy particles may be suspended against gravity in motion along closed trajectories. In reality, however, particles with a density different from the fluid cannot move in closed orbits due to the $\boldsymbol{u} \cdot \nabla \boldsymbol{u}$ term in (3.23); this will be clearly seen from the analysis to be carried out below. The absence of particle retention within a convection roll has been reported by Simon & Pomeau (1991), who carry out an experimental study of cellular flows similar to Bénard convection. To explain their observation that all heavy particles sink toward the bottom of the liquid layer, they first invoke (3.25). However, they do not identify particle inertia and fluid acceleration [the $\boldsymbol{u} \cdot \nabla \boldsymbol{u}$ term in (3.23)] as an agent which prevents the retention of particles by the convection rolls. Instead, they argue that molecular diffusion and small-scale fluctuations in the flow drive the particles which would otherwise be suspended for ever in closed orbits toward the lower hyperbolic points of Ψ_P, from which they move down and reach the bottom of the liquid layer. Equation (3.25) has also been used by Manton (1974) and Nielsen (1984) as the zeroth-order solution in their asymptotic analyses of particle motion in fluid flows generated by one vortex. For the first-order correction, Manton (1974) then introduces the effect of small particle inertia while Nielsen (1984) considers the effect of fluid acceleration.

Returning to our analysis, an integration of (3.24) will now be carried out. As all the terms in the right-hand side are evaluated at the instantaneous position of the particle, this integration will thus involve the evaluation of a line integral along the trajectory of the particle. Since to the first approximation the velocity of the particle is equal to the fluid velocity [see (3.23)], i.e. the trajectory of the particle is a streamline with perturbations occurring at $O(\gamma)$ and higher, we can perform the integration of (3.24) along the streamline which passes through the position of the particle at the begining of the integration, provided the time interval of integration is much smaller than $1/\gamma$. Note, however, that by integrating along a streamline instead of the trajectory of the particle, we can include only the leading term in the right-hand side of (3.24) since the incorporation of the higher-order terms would constitute a violation of the leading-order approximation. For convenience, we have chosen the integration period T as follows. For a particle outside the cat's eyes, the period T corresponds to the integration along a streamline over the entire horizontal span of a cat's eye; on the other hand, if the particle is inside a cat's eye, we integrate along half of a (closed) streamline from the rightmost to the leftmost positions, or vice versa, during the period T.

Denoting the change in Φ during one period T as $\Delta\Phi$, we thus have the following leading-order expression:

$$\Delta\Phi = \left(\tfrac{3}{2}\varepsilon - 1\right) \gamma \left[-\mathcal{F}(\Phi) + B\mathcal{G}(\Phi)\right], \tag{3.27}$$

where

$$\begin{aligned} \mathcal{F}(\Phi) &= \int_{t=t_0}^{t=t_0+T} \left[(\boldsymbol{u} \cdot \nabla u_y)\, u_x - (\boldsymbol{u} \cdot \nabla u_x)\, u_y\right] \mathrm{d}t \\ &= \int_{t=t_0}^{t=t_0+T} \frac{k\left(k \sin^2 x \cosh y + \cos x \sinh^2 y\right)}{(\cosh y - k \cos x)^3}\, \mathrm{d}t, \end{aligned} \tag{3.28}$$

and

$$\mathscr{G}(\Phi) = -\int_{t=t_0}^{t=t_0+T} u_x \, \mathrm{d}t. \tag{3.29}$$

Keeping in mind the argument in the last paragraph, it is understood that the integrals in (3.28) and (3.29) are evaluated along a streamline having the stream function Ψ equal to Φ. For an open streamline, the integration limits $(t = t_0, t = t_0 + T)$ correspond to $(x = -\pi, x = \pi)$ or $(x = \pi, x = -\pi)$ for a particle moving below or above the cat's eyes, respectively. If the particle is moving inside a cat's eye, we integrate from $x = x_{max}$ to $x = -x_{max}$ or vice versa, where $x_{max} > 0$ is the right intersection between the streamline and the x-axis. Physically, the meaning of (3.27) is as follows. Since the viscous drag is the dominant force acting on a particle, its trajectory, after the initial transient period of order γ, is a streamline except for a small perturbation. This perturbation, the magnitude of which after a period T is of order γ, is the combined effects of the gravitational force acting on the particle and its inertia, and results from the density difference between the particle and the fluid. For a neutrally buoyant particle, $\varepsilon = 2/3$, and $\Delta\Phi = 0$. The factor $\left(\frac{3}{2}\varepsilon - 1\right)$ has different signs for buoyant and heavy particles, and accounts for the fact that the effects of gravity and particle inertia on a buoyant particle are opposite to those on a heavy particle. For instance, gravity tends to deviate a buoyant particle from a streamline in the upward direction while it tends to pull a heavy particle downward away from the streamline. Owing to the inertial effects, a particle with a density different from the fluid cannot follow a curved streamline exactly. Thus, the function $\mathscr{F}$ accounts for the inertial-effect correction over the leading-order approximation of particle path being a streamline. Notice that $\mathscr{F}(\Phi)$ corrects for the cumulative effects of the inertial forces, $\boldsymbol{u} \cdot \nabla u_y$ and $\boldsymbol{u} \cdot \nabla u_x$, over the horizontal and vertical spans of the streamline segment, respectively. Moreover, since the curvature of the streamlines is, on average, in the direction of decreasing Ψ (see figure 1), and since a heavy particle cannot turn as much as a fluid element due to its greater inertia, we can expect that $\mathscr{F}(\Phi)$ is a positive quantity so that it has a positive contribution to $\Delta\Phi$ for heavy particles. This is indeed the case, as is confirmed by the $\mathscr{F}$–Φ plot in figure 2.

While (3.27) is convenient for the calculation of the change in Φ over one or a few periods, it may not be so if we are interested in the change in Φ over a large number of periods. For the long-time evolution of Φ, we can derive from (3.27) the approximate formula

$$\frac{\mathrm{d}\Phi}{\mathrm{d}\tau} = \left(\tfrac{3}{2}\varepsilon - 1\right) \frac{-\mathscr{F}(\Phi) + B\mathscr{G}(\Phi)}{T(\Phi)}, \tag{3.30}$$

where $\tau = \gamma t$ is the slow-time independent variable. In this paper, we are interested in the short-term evolution of Φ only. Equation (3.30) and the other aspects of the long-term evolution of Φ will be studied elsewhere.

To evaluate the integrals in (3.28) and (3.29), we first note that

$$\mathrm{d}t = \frac{\mathrm{d}x}{u_x} = \frac{\mathrm{d}y}{u_y}. \tag{3.31}$$

Substituting (3.31) into (3.28), we then obtain

$$\mathscr{F}(\Phi) = 2k\mathrm{e}^{-2\Phi} \int_0^{\pi} \frac{k \sin^2 x \cosh y + \cos x \sinh^2 y}{\sinh y} \, \mathrm{d}x \tag{3.32}$$

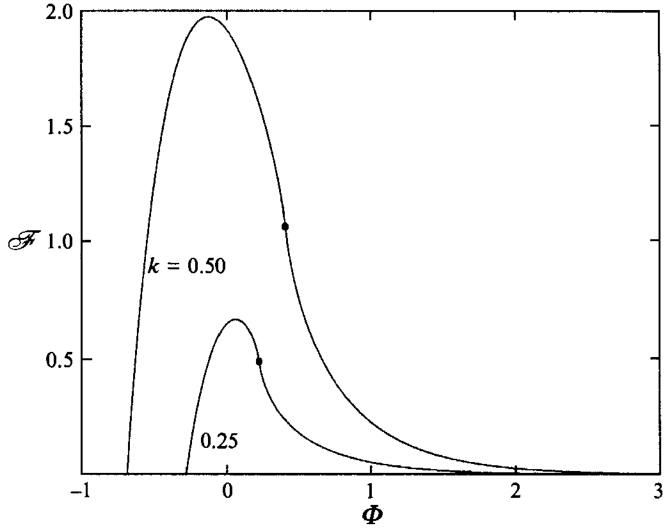

FIGURE 2. The function $\mathscr{F}(\Phi)$ with parameter $k = 0.25, 0.50$. The symbol • denotes the boundary of a cat's eye.

with

$$\cosh y = \mathrm{e}^{\Phi} + k\cos x, \qquad y \geqslant 0. \tag{3.33}$$

Equation (3.32) is valid for $\Phi \geqslant \Psi_{cr}$, where Ψ_{cr} is the stream function at the separatrix (i.e. boundary) of a cat's eye and is given by

$$\Psi_{cr} = \ln(1+k). \tag{3.34}$$

For particles inside a cat's eye, $\Phi < \Psi_{cr}$, we have

$$\mathscr{F}(\Phi) = 2k\mathrm{e}^{-2\Phi} \int_0^{x_{max}} \frac{k\sin^2 x \cosh y + \cos x \sinh^2 y}{\sinh y}\, \mathrm{d}x \tag{3.35}$$

with

$$\cos x_{max} = \frac{1-\mathrm{e}^{\Phi}}{k}, \qquad 0 < x_{max} < \pi, \tag{3.36}$$

and y given by (3.33). Note that $\mathscr{F}(\Phi)$ is independent of whether a particle is moving above or below the x-axis, reflecting the fact that the streamlines are symmetric with respect to this axis (see figure 1). From (3.29), we obtain

$$\mathscr{G}(\Phi) = \begin{cases} 2x_{max}\,\mathrm{sign}\,(y) & \text{if } \Phi < \Psi_{cr} \\ 2\pi\,\mathrm{sign}\,(y) & \text{if } \Phi \geqslant \Psi_{cr} \end{cases} \tag{3.37}$$

with x_{max} as given in (3.36). Thus, $\mathscr{G}(\Phi)$ is positive for a particle which is located above the x-axis at the begining of the period T, and is negative if the particle is initially below the x-axis. This antisymmetric behaviour of $\mathscr{G}(\Phi)$ follows from the fact that gravity is unidirectional. For instance, a bubble located above the x-axis experiences an upward push away from the axis, resulting in an increase in Φ; on the other hand, this upward force will push a bubble located below the x-axis toward a smaller Φ.

In figure 2, we plot the function $\mathscr{F}$ versus Φ with k as a parameter. The behaviour of the function $\mathscr{G}$ with respect to Φ is depicted in figure 3. It should be observed from

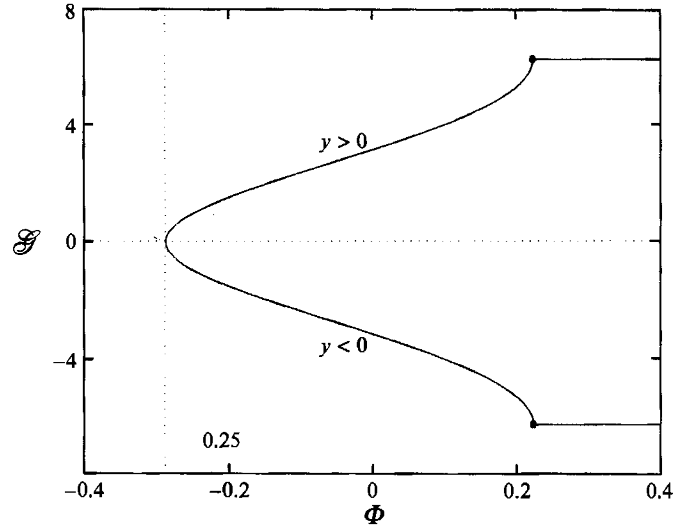

FIGURE 3. The function $\mathscr{G}(\Phi)$ with $k = 0.25$. The symbol • denotes the boundary of a cat's eye.

these figures that if a particle makes one complete loop along a closed streamline, $\mathscr{F}(\Phi)$ always has a non-zero contribution to the change in the 'particle path function' but the net contribution from $\mathscr{G}(\Phi)$ is always zero. It then follows from (3.27) that a particle with a mass density different from the fluid cannot stay in motion along a closed trajectory. This conclusion is consistent with the asymptotic analyses of Manton (1974) and Nielsen (1984). Having calculated the functions $\mathscr{F}(\Phi)$ and $\mathscr{G}(\Phi)$, we are now in the position to examine some interesting aspects of particle motion in the Stuart vortex flow. First, let us define the function

$$\mathscr{H} \equiv [-\mathscr{F}(\Phi) + B\mathscr{G}(\Phi)] \operatorname{sign}\left(\tfrac{3}{2}\varepsilon - 1\right) \tag{3.38}$$

so that

$$\Delta\Phi = \gamma \left|\tfrac{3}{2}\varepsilon - 1\right| \mathscr{H}. \tag{3.39}$$

Now, we can examine the dynamics of heavy particles and buoyant particles. We will do this separately.

3.1. *Heavy particles*

For heavy particles, i.e. $\varepsilon < 2/3$, the behaviour of the function $\mathscr{H}$ is as sketched in figure 4. Notice that there are two equilibrium points (such that $\Delta\Phi = 0$). The first one, $\Phi = \Psi_0$, is the centre of a vortex, and is clearly seen to be unstable. The second one, $\Phi = \Psi_e$, is stable. This stable equilibrium point corresponds to particle suspension in an open periodic trajectory located above the vortices. In figure 5, the equilibrium stream function Ψ_e is plotted as a function of B with k being a parameter. For a fixed value of k, observe from figure 5 that as B increases, the stable particle trajectory shifts down toward the x-axis, since Ψ_e decreases in response to an increase in B. Finally, if B is increased to the critical value of $\mathscr{F}(\Psi_{cr})/2\pi$, then Ψ_e coincides with Ψ_{cr} and no particles can be suspended any longer so that all settle under the pull of gravity. In figure 6, this threshold value of B for the existence of particle suspensions is plotted as a function of k. As expected, it increases with k.

The suspension of heavy particles above the Stuart vortices has been observed in the numerical study of Gañán-Calvo & Lasheras (1991). In fact, our observation

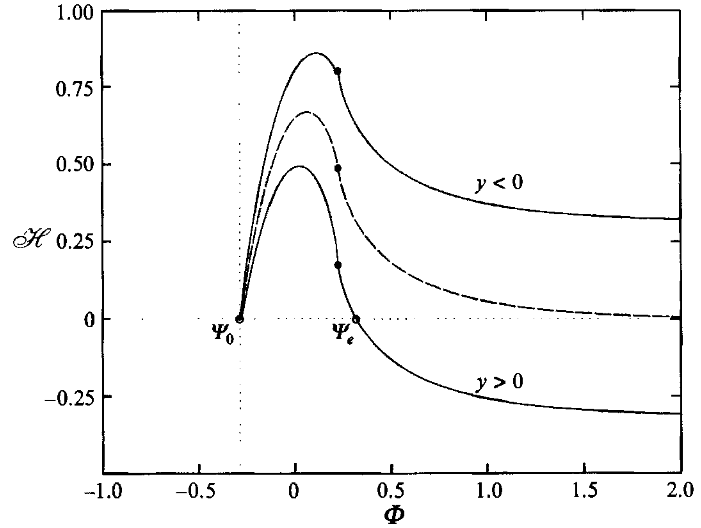

FIGURE 4. The function $\mathscr{H}(\Phi)$ for heavy particles. Here, $k = 0.25$ and $B = 0.05$. The dashed curve is the function $\mathscr{F}(\Phi)$, and the symbol • designates the boundary of a cat's eye. Ψ_0 and Ψ_e are the equilibrium points.

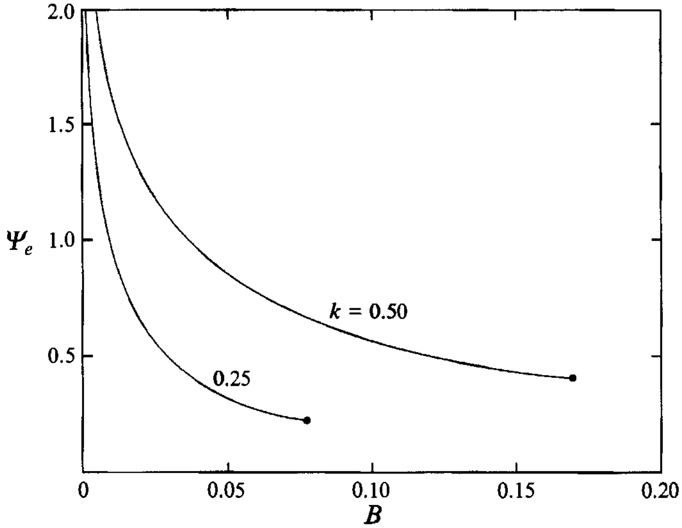

FIGURE 5. The equilibrium stream function Ψ_e as a function of B with k being a parameter. The symbol • corresponds to the boundary of a cat's eye, so that $\Psi_e = \Psi_{cr}$ and $B = \mathscr{F}(\Psi_{cr})/2\pi$.

here of particle trajectories being shifted down toward the x-axis as B increases is consistent with their findings. However, our approximate analysis based on dominant viscous drag cannot predict the existence of the quasi-periodic and chaotic trajectories observed in their study. This is so because the assumption of small γ effectively reduces the four-dimensional dynamical system of (2.10)–(2.13) to that of two dimensions given by (3.23). Furthermore, this reduced dynamical system is autonomous, and chaos is thus non-existent.

As can be seen from figure 4, a particle initially moving above the trajectory associated with the equilibrium point $\Phi = \Psi_e$ will asymptotically converge to this stable trajectory. The same outcome can also be easily seen for a particle initially

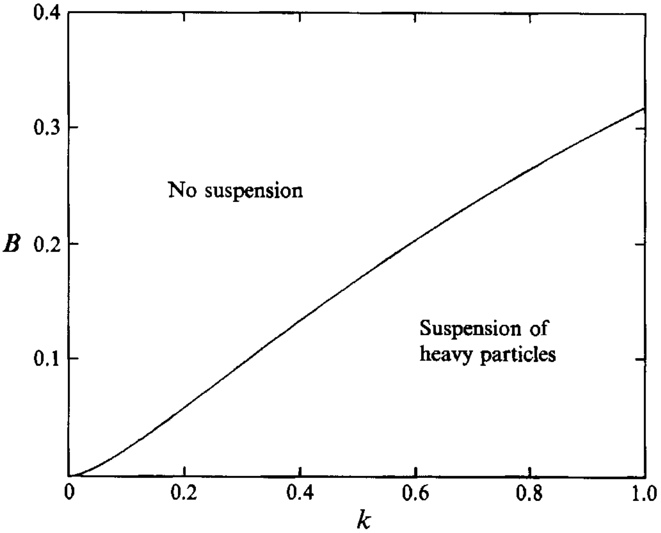

FIGURE 6. Threshold values of B as a function of k for the existence of the suspension of heavy particles.

located between the asymptotic trajectory and the separatrix. For particles moving very near the separatrix, either inside or outside a cat's eye, a simple map can be derived from (3.27). In this case, we first note that $\mathscr{F}(\Phi) \approx \mathscr{F}_{cr}$, where $\mathscr{F}_{cr}$ is equal to $\mathscr{F}(\Psi_{cr})$, and $\mathscr{G}(\Phi) \approx 2\pi \mathrm{sign}(y)$. Then, (3.27) reduces to

$$\Phi_{j+1} - \Phi_j = \left(\tfrac{3}{2}\varepsilon - 1\right)\gamma\left[-\mathscr{F}_{cr} + 2\pi B\ \mathrm{sign}(y)\right], \tag{3.40}$$

where Φ_j is the 'particle path function' at the beginning of a period, and Φ_{j+1} is equal to Φ evaluated at the end of that period (or the beginning of the next period). Introducing the rescaled variable

$$\tilde{\Phi}_i \equiv \frac{\Phi_i - \Psi_{cr}}{\left(1 - \frac{3}{2}\varepsilon\right)\gamma}, \tag{3.41}$$

which has been stretched with the factor of $1/\left(1 - \frac{3}{2}\varepsilon\right)\gamma$, into (3.40), we then obtain the following map:

$$\tilde{\Phi}_{j+1} = \tilde{\Phi}_j + \left[\mathscr{F}_{cr} - 2\pi B\ \mathrm{sign}(y)\right]. \tag{3.42}$$

It should be noted that the $\tilde{\Phi}_i$ associated with a particle outside the cat's eyes is positive, while $\tilde{\Phi}_i$ takes on a negative value if the particle is moving inside a cat's eye.

In figures 7 (*a*), 7 (*b*) and 7 (*c*), the linear map given by (3.42) is shown for the case of $2\pi B < \mathscr{F}_{cr}$. In this case, there exists a stable equilibrium point Ψ_e satisfying the equation

$$\mathscr{F}(\Psi_e) = 2\pi B \tag{3.43}$$

(see figure 4). All particles initially moving above the Stuart vortices will asymptotically converge to the stable trajectory associated with Ψ_e. In fact, as can be seen from figures 7 (*a*), 7 (*b*) and 7 (*c*), even particles initially moving inside a cat's eye will converge to this asymptotic path, provided they are located above the x-axis and sufficiently close to the separatrix, i.e. $\tilde{\Phi} > \tilde{\Phi}_L = 2\pi B - \mathscr{F}_{cr}$. As an illustration, consider a particle initially inside a cat's eye and represented by point 1 in figure 7 (*a*). Since the effect of gravity, which tends to pull the particle downward, is not strong enough, after one period T the particle ends up at position 2 outside the separatrix.

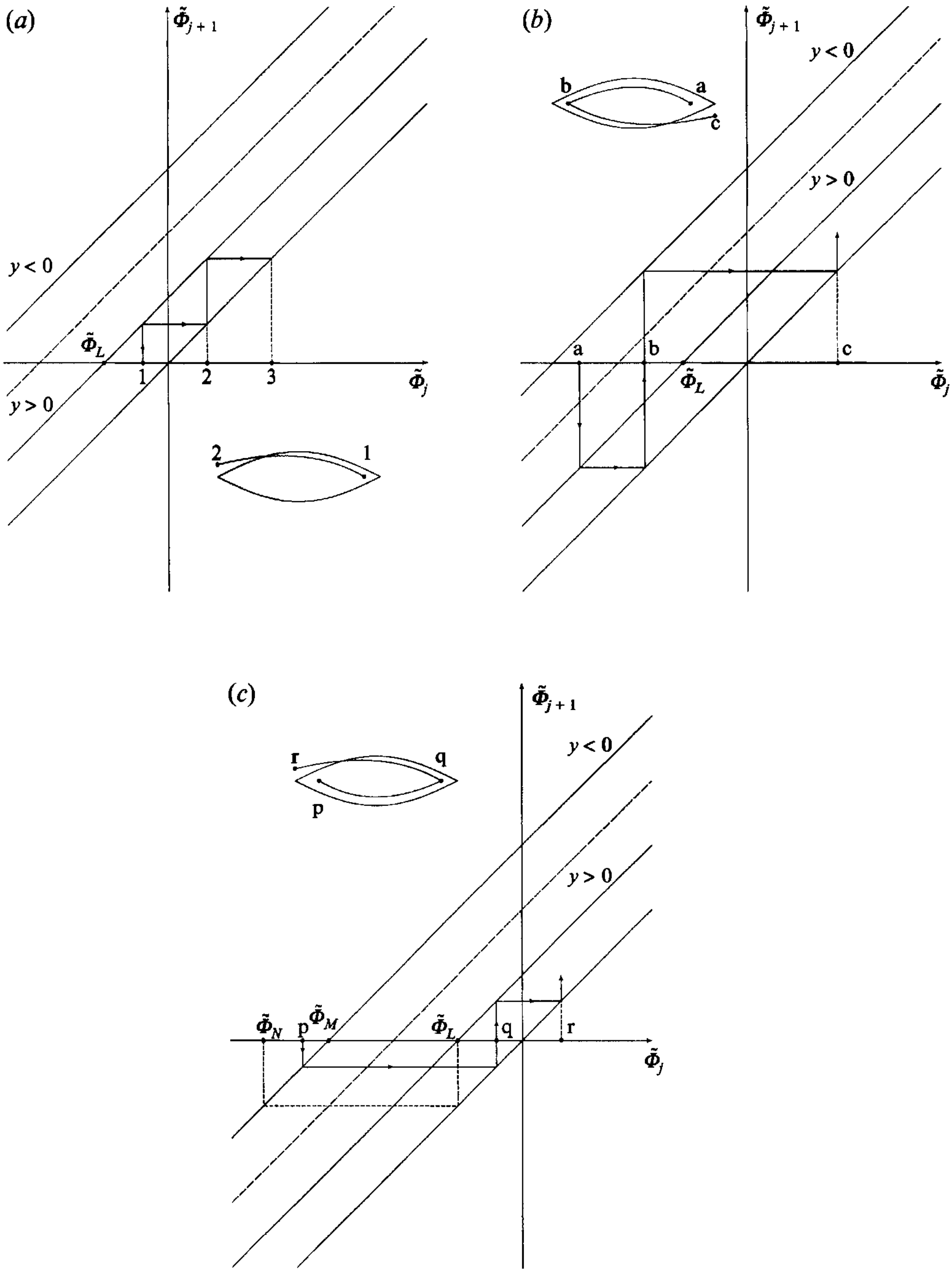

FIGURE 7. The maps for the motion of a heavy particle in the vicinity of the boundary of a cat's eye, equation (3.42). Here, $2\pi B < \mathcal{F}_{cr}$. For clarity, each map is accompanied by an insert consisting of the cat's eye and a sketch for the corresponding motion in the physical space.

After this, the particle asymptotically converges to the stable trajectory given by the equilibrium point Ψ_e. However, if initially the particle is sufficiently far away from the separatrix, it may escape the cat's eye from below and eventually settle to $y = -\infty$, as is clearly shown by the successive positions a, b, and c in figure 7 (*b*). For particles

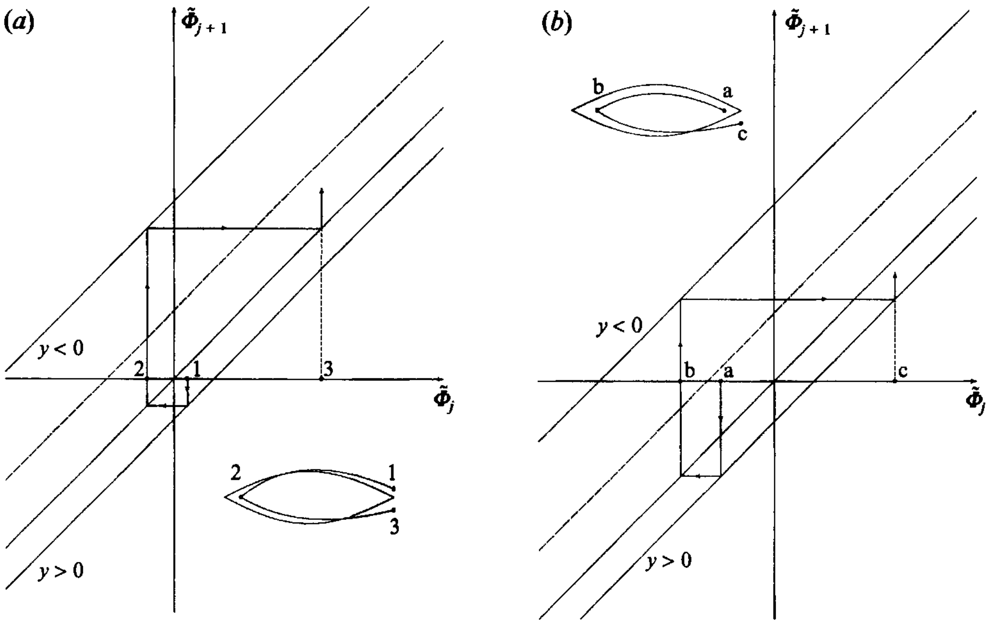

FIGURE 8. The maps for a heavy particle, equation (3.42), with $2\pi B > \mathscr{F}_{cr}$.

initially moving inside a cat's eye and below the x-axis, they either escape the cat's eye from above and converge to the asymptotic trajectory given by Ψ_e, or fall out of the cat's eye from below and eventually settle to $y = -\infty$, depending on their initial $\tilde{\Phi}$. As illustrated by the p-q-r sequence of locations in figure 7 (c), particles initially in the range of $\tilde{\Phi}_N < \tilde{\Phi} < \tilde{\Phi}_M$, where $\tilde{\Phi}_M = -(\mathscr{F}_{cr} + 2\pi B)$ and $\tilde{\Phi}_N = -2\mathscr{F}_{cr}$, escape the cat's eye from above after making one complete loop. If their initial $\tilde{\Phi}$ is greater than $\tilde{\Phi}_M$, they are too close to the separatrix and, at the end of the period, fall out of the cat's eye from below. Finally, if their initial $\tilde{\Phi}$ is smaller than $\tilde{\Phi}_N$, they will still be moving inside the cat's eye after making one complete loop; eventually, they either converge to the asymptotic trajectory located above the cat's eye or settle to $y = -\infty$, depending on the initial values of $\tilde{\Phi}$.

In the case of $2\pi B > \mathscr{F}_{cr}$, the map given by (3.42) is shown in figures 8 (a) and 8 (b). In this case, the gravitational effect is too strong for any particle suspension to exist, and all particles settle to $y = -\infty$. The sequence of positions 1-2-3 illustrates how a particle enters a cat's eye from above and ecapes from below, while the sequence of a-b-c shows the escape of a particle initially inside a cat's eye.

3.2. *Buoyant particles*

For buoyant particles, $\varepsilon > 2/3$, and the function $\mathscr{H}(\Phi)$ is simply the negative of the corresponding $\mathscr{H}$ for heavy particles [see (3.38)]. From figure 4, we see that there are also two equilibrium points (or streamlines) for buoyant particles: $\Phi = \Psi_e$ and $\Phi = \Psi_0$. The first one is unstable. The second one, which in the leading-order approximation is the centre of a vortex, is stable. A consequence of the existence of stable equilibrium points is that depending on their initial position and velocity, buoyant particles may be trapped inside the vortices and coalesce at the equilibrium points. However, it is clear that particles released above and sufficiently far away from the vortices will not be trapped; instead, they will escape to $y = \infty$. If the particles are released above but close to the cat's eyes, they may be captured by the vortices, as

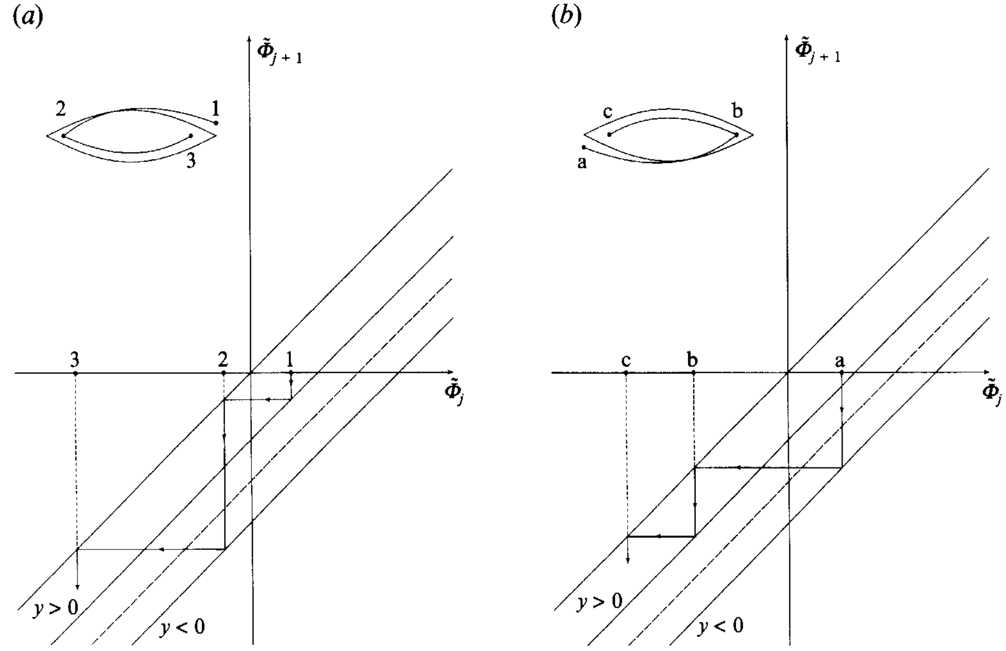

FIGURE 9. The maps for a buoyant particle, equation (3.44), with $2\pi B < \mathscr{F}_{cr}$.

will be seen later. For particles released below the cat's eyes, their evolution dynamics consist of convection by the bulk flow and the vertical rise due to buoyancy force, so that they will eventually enter the vortices. What happens after a particle enters a cat's eye: will it remain trapped there, or will it escape from captivity? To answer this question, we need to derive a map similar to that given in (3.42).

For buoyant particles moving very close to the separatrix of the cat's eyes, the counterpart of (3.42) is the map

$$\tilde{\Phi}_{j+1} = \tilde{\Phi}_j + [-\mathscr{F}_{cr} + 2\pi B \,\mathrm{sign}\,(y)], \tag{3.44}$$

where $\tilde{\Phi}_i$ is defined by

$$\tilde{\Phi}_i \equiv \frac{\Phi_i - \Psi_{cr}}{\left(\frac{3}{2}\varepsilon - 1\right)\gamma}. \tag{3.45}$$

Note that by using the definition given by (3.45) instead of (3.41), we have preserved the convention that $\tilde{\Phi}_i$ is positive for a particle outside the separatrix and negative if the particle is moving inside a cat's eye.

In figures 9 (*a*) and 9 (*b*), we show the maps given in (3.44) for the case of $2\pi B < \mathscr{F}_{cr}$. As can be seen from figure 4, there exists an unstable equilibrium point Ψ_e satisfying equation (3.43). All particles moving in the upper half-space with initial 'particle path functions' greater than Ψ_e will eventually escape to $y = \infty$. On the other hand, if initially $\Phi < \Psi_e$, a particle will gradually approach and enter a cat's eye from above. As is evidently illustrated by the steps 1-2-3 in figure 9 (*a*), once a buoyant particle enters a cat's eye from above, it will remain trapped there, spiralling toward the stable equilibrium point located inside the vortex. For particles entering a cat's eye from below, they experience the same outcome, as illustrated by the steps a-b-c in figure 9(*b*).

When $2\pi B > \mathscr{F}_{cr}$, the effect of buoyancy is strong enough so that all particles

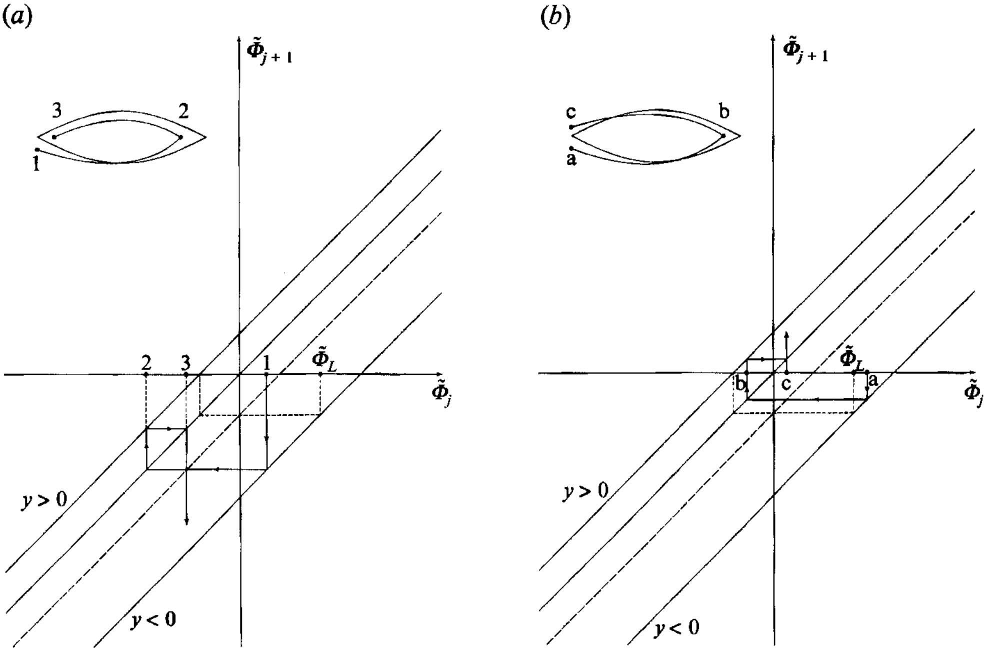

FIGURE 10. The maps for a buoyant particle, equation (3.44), with $2\pi B > \mathscr{F}_{cr}$.

initially moving above the vortices will escape to $y = \infty$. Particles entering a cat's eye from below may remain trapped inside the vortex, provided they move sufficiently quickly away from the separatrix once they enter the cat's eye; however, if they stay sufficiently close to the separatrix after entering, they may escape from the vortex, eventually moving to $y = \infty$. These two scenarios for particles entering a cat's eye from below are illustrated in figures 10(*a*) and 10(*b*). Observe that for a particle to enter a cat's eye and escape, $\tilde{\Phi}_L \leqslant \tilde{\Phi}_a < \mathscr{F}_{cr} + 2\pi B$, where $\tilde{\Phi}_L = 2\mathscr{F}_{cr}$. For a particle to enter a cat's eye from below and remain trapped there, $0 < \tilde{\Phi}_1 < \tilde{\Phi}_L$. Assuming a Stuart vortex flow with a uniform/continuous distribution of buoyant particles, we can, using figures 10(*a*) and 10(*b*), estimate the fraction of the particles which enter a cat's eye from below and remain trapped by the vortex. In fact, we can easily derive a formula for the trapped fraction of the entering particles, fr, as

$$fr = \frac{2\mathscr{F}_{cr}}{\mathscr{F}_{cr} + 2\pi B}. \tag{3.46}$$

4. Equilibrium points

From the analysis of dominant viscous drag in the last section, we see that buoyant particles may be trapped by a vortex and spiral toward the central region, and that heavy particles always recede from the centre of the vortex. In this section, we shall attempt to see if these phenomena of entrapment/non-entrapment of buoyant/heavy particles still persist in the more general cases where the viscous drag is not necessarily the dominant force. Thus, we now relax the condition of $A \gg 1$, and perform a numerical study of the equilibrium point(s) of the dynamical system given by

(2.10)–(2.13). First, we write

$$\frac{\mathrm{d}x}{\mathrm{d}t} = F_1\left(x,y,V_x,V_y\right) = V_x, \tag{4.1}$$

$$\frac{\mathrm{d}y}{\mathrm{d}t} = F_2\left(x,y,V_x,V_y\right) = V_y, \tag{4.2}$$

$$\frac{\mathrm{d}V_x}{\mathrm{d}t} = F_3\left(x,y,V_x,V_y\right) = \tfrac{3}{2}\varepsilon \boldsymbol{u}\cdot\nabla u_x + \left(u_x - V_x\right)Af_{\mathrm{d}}, \tag{4.3}$$

$$\frac{\mathrm{d}V_y}{\mathrm{d}t} = F_4\left(x,y,V_x,V_y\right) = \tfrac{3}{2}\varepsilon \boldsymbol{u}\cdot\nabla u_y + \left(u_y - V_y\right)Af_{\mathrm{d}} + \left(\tfrac{3}{2}\varepsilon - 1\right)B. \tag{4.4}$$

Then, the equilibrium point is given by $\left(x,y,V_x,V_y\right)_{equi} = (\bar{x},\bar{y},0,0)$, where $(\bar{x},\bar{y})$ satisfies the simultaneous equations

$$\left.\begin{aligned} f_3(\bar{x},\bar{y}) &\equiv F_3(\bar{x},\bar{y},0,0) = 0, \\ f_4(\bar{x},\bar{y}) &\equiv F_4(\bar{x},\bar{y},0,0) = 0. \end{aligned}\right\} \tag{4.5}$$

That is, $(\bar{x},\bar{y})$ is given by the intersection(s) of the two curves $f_3(x,y) = 0$ and $f_4(x,y) = 0$ in the (x,y)-plane. From the theory of dynamical systems, it is well known that the equilibrium point $(\bar{x},\bar{y},0,0)$ is asymptotically stable if all the eigenvalues of the Jacobian matrix associated with the system of (4.1)–(4.4) have negative real parts. For simplicity, we will assume that f_d is a constant when we take the derivatives of F_3 and F_4. Under this simplification, we then obtain the characteristic equation for the eigenvalue ξ as

$$\xi^2(Af_d+\xi)^2 - \left(\frac{\partial f_3}{\partial x} + \frac{\partial f_4}{\partial y}\right)\xi(Af_d+\xi) + \left(\frac{\partial f_3}{\partial x}\frac{\partial f_4}{\partial y} - \frac{\partial f_3}{\partial y}\frac{\partial f_4}{\partial x}\right) = 0, \tag{4.6}$$

where f_d and the derivatives of f_3 and f_4 are evaluated at the equilibrium point. The solutions of (4.6) is given by

$$\xi = -\frac{1}{2}Af_d\left[1 \pm \left(1 + \frac{2\mathscr{D}}{(Af_d)^2}\right)^{\frac{1}{2}}\right], \tag{4.7}$$

where

$$\mathscr{D} = \left(\frac{\partial f_3}{\partial x} + \frac{\partial f_4}{\partial y}\right) \pm \left[\left(\frac{\partial f_3}{\partial x} - \frac{\partial f_4}{\partial y}\right)^2 + 4\frac{\partial f_3}{\partial y}\frac{\partial f_4}{\partial x}\right]^{\frac{1}{2}}. \tag{4.8}$$

In the following discussion, we use formula (4.7) to determine the stability of the fixed points.

We begin with buoyant particles. Figure 11 is an illustration of the case in which B varies while the other four parameters are kept constant. For this particular set of the four parameters k, Re, A, and ε, there exist two equilibrium points for each $B < 6.484$: the one to the left is unstable while the right one is stable. Throughout this paper, we follow the convention of representing stable equilibrium points with solid lines and designating unstable fixed points with dashed lines. That only one of the two fixed points is stable is consistent with our numerical simulations of the motion of buoyant particles. Here, it is found that all particles which do not escape to $y = \infty$ are trapped by the vortices at a single point inside each vortex. Returning to figure 11, when $B = 0$, the stable equilibrium point is located at $(\bar{x} = 0, \bar{y} = 0)$ and the unstable fixed point at $(\bar{x} = -\pi, \bar{y} = 0)$. As B increases, the two equilibrium

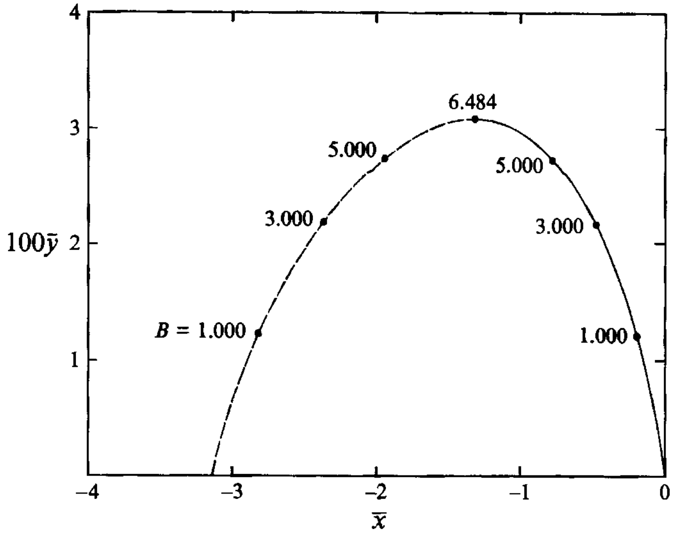

FIGURE 11. Loci of the equilibrium points of the dynamical system of (2.10)–(2.13). Here, we vary B while holding the other parameters fixed at $k = 0.25$, $Re = 100.0$, $A = 5.0$, and $\varepsilon = 1.0$. The solid curve represents stable fixed points while the unstable equilibrium points are designated by the dashed curve.

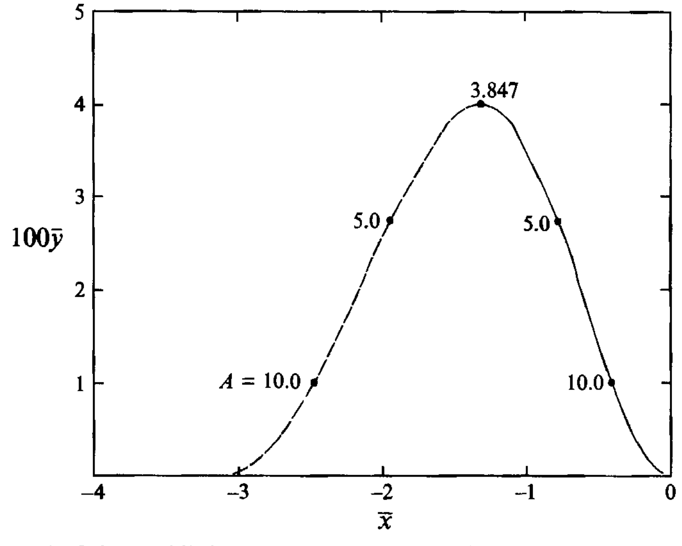

FIGURE 12. Loci of the equilibrium points of the dynamical system of (2.10)–(2.13) generated by varying A while keeping the other parameters fixed at $k = 0.25$, $Re = 100.0$, $B = 5.0$, and $\varepsilon = 1.0$.

points become closer until they collide with each other when B reaches the value of 6.484. Further increase in B results in the disappearance of the equilibrium points. Physically, this means that the buoyancy forces acting on the particles are now so strong that the vortices can no longer capture any particle. In the terminology of dynamical systems theory, the equilibrium points of figure 11 undergo a saddle-node bifurcation at $B = 6.484$: for $B < 6.484$ there are two equilibrium points, while no fixed point exists for $B > 6.484$.

In figure 12, we vary the parameter A while holding the other four constant. For

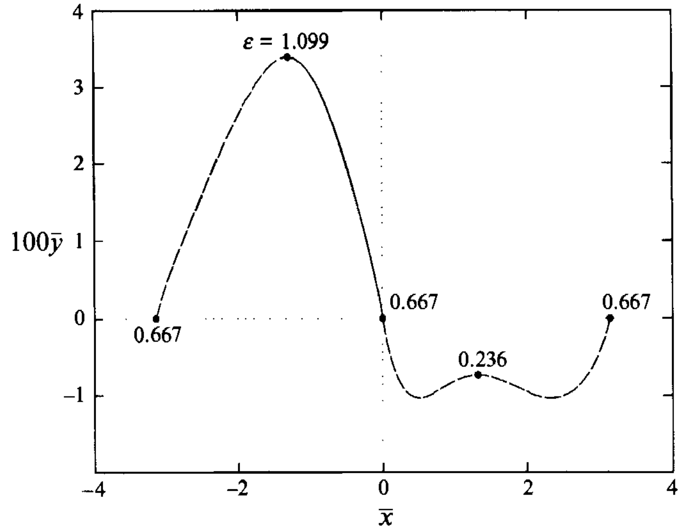

FIGURE 13. The equilibrium points of the dynamical system of (2.10)–(2.13) for heavy and buoyant particles. Here, $k = 0.25$, $Re = 100.0$, $A = 5.0$, $B = 5.0$ while ε varies from $\varepsilon = 0.236$ to $\varepsilon = 1.099$.

this particular choice of fixed k, Re, B, and ε, the equilibrium points undergo a saddle-node bifurcation at $A = 3.8467$. For all values of A smaller than 3.8467, the viscous drag on the particles is not large enough to counteract the buoyancy force, and all particles escape to $y = \infty$. When A is greater than the bifurcation value of 3.8467, there exists a stable equilibrium point (in addition to an unstable fixed point) inside each vortex, and all particles captured by the vortex eventually converge to this equilibrium point. As A increases, i.e. as the viscous drag force becomes more dominant, the stable and unstable fixed points move toward the centre of the vortex and the tip of the cat's eye, respectively, where the fluid velocity is zero. Note that the movement of the stable equilibrium point toward the vortex centre as A increases is consistent with the analysis based on dominant viscous drag forces carried out in §3, where the vortex centre becomes the stable equilibrium point in the limit of $A \rightarrow \infty$.

Figure 13 depicts the evolution of the equilibrium points as the density ratio is varied, covering both heavy and buoyant particles. For the four constant parameters k, Re, A, and B chosen here, no equilibrium point exists for $\varepsilon < 0.2358$. Apparently, the particles are so heavy that gravity cannot be balanced out by the other forces acting on the particles. When ε is increased beyond the value of 0.2358, two equilibrium points appear in the lower-right quadrant of a cat's eye for each $\varepsilon < 2/3$. However, both of these fixed points are unstable, in consistence with the analysis of §3, which predicts that heavy particles can be suspended only in motion along a periodic open trajectory located above the vortices. When ε is increased to the value of 2/3, the left branch of the locus reaches the vortex centre and the equilibrium point becomes stable; on the other hand, the right branch reaches the right-hand tip of the cat's eye, but no change in stability ever takes place. When ε is increased further, we enter the range of buoyant particles, and the left branch becomes a stable locus while the right branch continues as the locus of unstable equilibrium points, starting at the left-hand tip of the cat's eye. Finally, when ε reaches the value of 1.099, the two loci collide with each other. Further increase in ε results in the

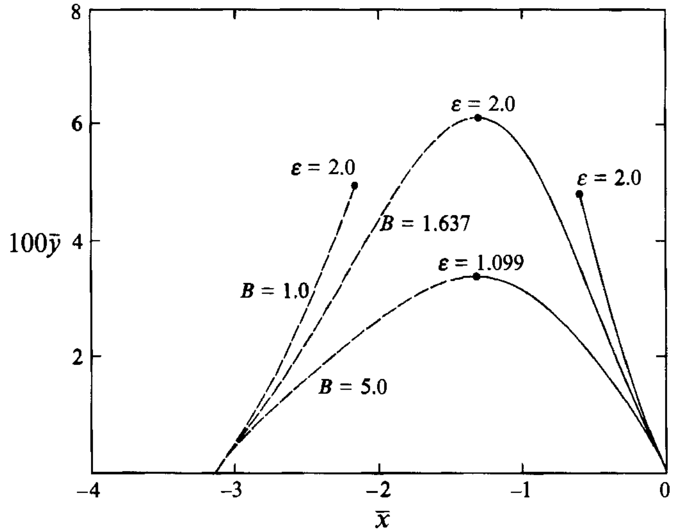

FIGURE 14. The evolution of the loci for buoyant particles in figure 13 in response to a decrease in B. The three parameters k, Re, and A are kept constant.

disappearance of the equilibrium points, corresponding to the situation of no particle entrapment.

In figure 14, we show how the two loci for buoyant particles in figure 13 evolve in response to changes in the gravity parameter B (while k, Re, and A are kept constant). As B decreases from the value of 5.0, the bifurcation value of ε increases from 1.099, signifying that particles which were previously too light to be captured by the vortices may now be trapped. When B decreases to the value of 1.637, the bifurcation value reaches the bubble limit of $\varepsilon = 2$. Thus, for $B < 1.637$, the whole range of particles, from neutrally buoyant particles to bubbles, can be suspended in the flow, held in captivity by the stable equilibrium points. Note that for each $B < 1.637$, the stable and unstable loci of equilibrium points do not collide at a bifurcation point; instead, they form two distinct branches, each covering the whole range of $2/3 \leqslant \varepsilon \leqslant 2$. This is clearly illustrated by the case of $B = 1.0$ in the figure.

To conclude our discussion on the equilibrium points, let us summarize the main points of this section. When the gravitational force is sufficiently small, there exists a stable equilibrium point for buoyant particles inside a Stuart vortex so that they may remain at rest there; on the other hand, the equilibrium point becomes unstable in the case of heavy particles and, consequently, they always recede away from it. That the equilibium point is stable for buoyant particles but unstable for heavy particles is always true, regardless of the strength of the viscous drag, and seems to be a general feature of particle motion in vortical flows. In particular, it has also been observed in Langmuir cellular flows (Maxey 1987; Crisanti *et al.* 1990) and in solid-rotation vortices (Nielsen 1984).

5. Results of numerical simulations

In this section, we discuss the results obtained by integrating numerically the dynamical system of (2.10)–(2.13). Our main objective here is to ascertain the accuracy of the asymptotic model discussed in §3. To this end, we will compare its predictions with the results of numerical integration. In this section, we will also

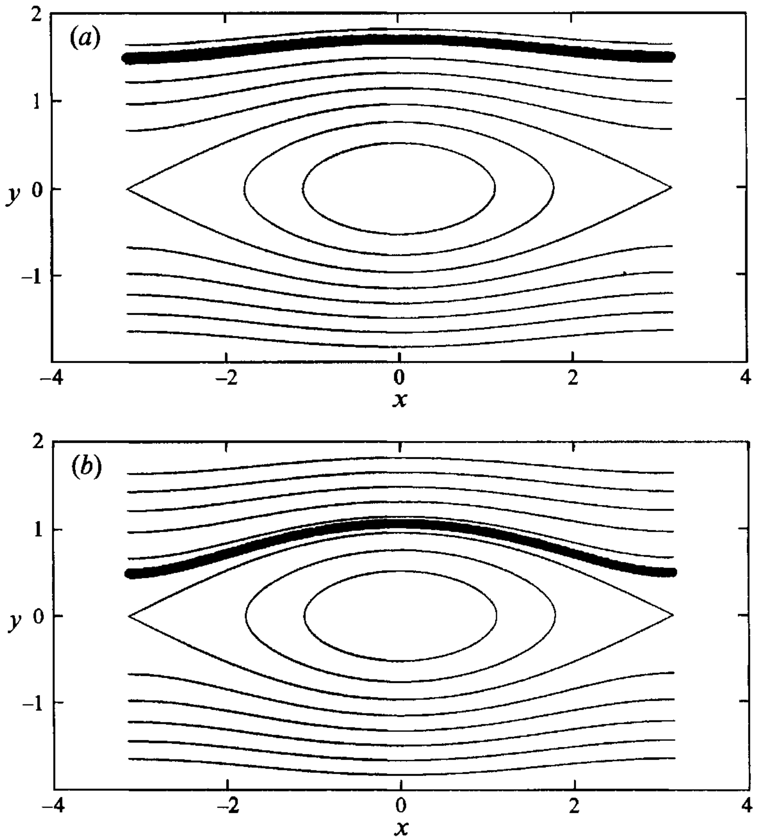

FIGURE 15. Asymptotic solutions of the dynamical system of (2.10)–(2.13), along which heavy particles which remain suspended at large times move. The parameters are: $k = 0.25$, $Re = 50.0$, $A = 50.0$, $\varepsilon = 0.05$, and (*a*) $B = 0.01$; (*b*) $B = 0.05$.

investigate the dependence on the five parameters k, Re, A, B, and ε of the dynamics of particles in Stuart vortex flows when the viscous drag is not necessarily dominant. In this case, we will focus on buoyant particles only, since the dynamics of heavy particles have been studied extensively (Gañán-Calvo & Lasheras 1991; Tio *et al.* 1993*a*).

For the purpose of accurate integration, we have chosen the fourth-order Runge–Kutta scheme with a time step of 0.01. The accuracy of this time step is examined by integrating the system of (2.10)–(2.13) in several test cases; in particular, we are able to obtain the open and closed streamlines of the flow field. For the initial conditions, we choose the initial velocity of the particles to be that of the fluid elements at the initial position of the particles. Unless stated otherwise, this is the initial condition used in our computations.

We begin with heavy particles. Figures 15(*a*) and 15(*b*) show the asymptotic solution (trajectory) of the dynamical system of (2.10)–(2.13), to which the trajectories of all particles which remain suspended in the flow converge. Figure 15(*a*) is a snapshot at large time of the position of 1235 particles moving along the asymptotic trajectory while there are 1103 particles occupying the segment of the trajectory shown in figure 15(*b*). In both cases, the trajectories are periodic, the period being equal to 2π. Note that we have selected a fairly large value for the parameter A, so that

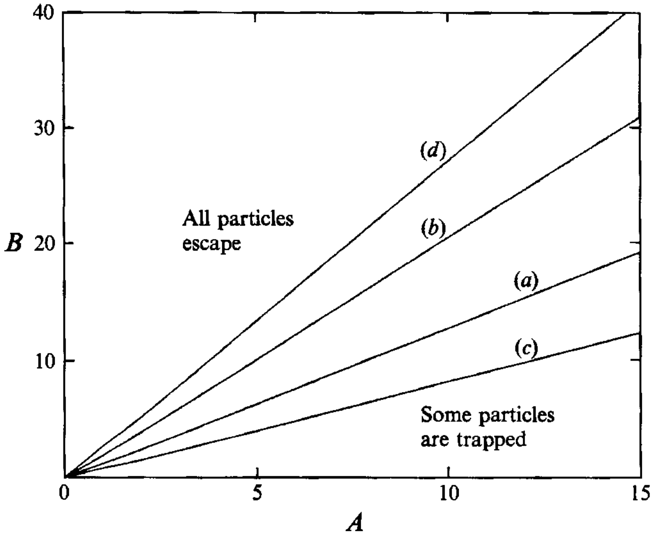

FIGURE 16. Regions of entrapment/non-entrapment of buoyant particles in the subsets of the parametric space with (*a*) $k = 0.25$, $Re = 100.0$, $\varepsilon = 1.0$; (*b*) $k = 0.25$, $Re = 300.0$, $\varepsilon = 1.0$; (*c*) $k = 0.25$, $Re = 300.0$, $\varepsilon = 1.5$; (*d*) $k = 0.50$, $Re = 300.0$, $\varepsilon = 1.5$.

comparison can be made with the analysis of §3, which is based on the assumption of dominant viscous drag forces. Also, the gravity parameter has been chosen to be $B < \mathscr{F}(\Psi_{cr})/2\pi \approx 0.080$. We recall from the discussion in §3 that for suspension of heavy particles to exist, it is required that $B < \mathscr{F}(\Psi_{cr})/2\pi$ (see figures 5 and 6). In fact, in a separate simulation with $B = 0.1$ and the other four parameters identical to those of figures 15 (*a*) and 15 (*b*), it is observed that all particles settle toward $y = -\infty$. Also, observe from figures 15 (*a*) and 15 (*b*) that an increase in the parameter B results in a downward shift of the asymptotic trajectory, in accordance with the prediction of §3 (see figure 5). Quantitatively, the numerical results and analytical predictions are also in good agreement. For example, the 'particle path function' of the particles shown in figure 15 (*a*) yields an average value of $\Phi_{ave} \approx 0.958$ while the prediction of §3 (see figure 5) gives a value of $\Psi_e \approx 0.957$ for the equilibrium stream function. For the particles shown in figure 15 (*b*), $\Phi_{ave} \approx 0.319$ while the calculation of figure 5 gives a value of $\Psi_e \approx 0.318$. For a more detailed discussion on heavy particles, the reader is referred to the papers of Gañán-Calvo & Lasheras (1991) and Tio *et al.* (1993*a*). In the remaining part of this section, we will focus our attention on buoyant particles only.

Depending on the values of the five parameters k, Re, A, B, and ε, the motion of buoyant particles in the Stuart vortex flow can be broadly classified into two scenarios. In the first scenario, some particles are captured by the vortices and remain trapped at the stable equilibrium points while the others escape to $y = \infty$. Whether a particle is trapped or escapes to $y = \infty$ depends on the initial position and velocity of the particle. In the second scenario, not a single particle is trapped by the vortices. Instead, all particles escape to $y = \infty$.

Figure 16 shows the regions of entrapment/non-entrapment of buoyant particles in the subsets (with fixed k, Re, and ε) of the parametric space. For each of the four cases represented by (*a*), (*b*), (*c*), and (*d*), the corresponding curve denotes the boundary between the regions of entrapment and non-entrapment of buoyant particles. Let us begin with case (*a*). For a non-zero value of A, say 5.0, and a sufficiently small B, particles which do not escape to $y = \infty$ are trapped by the vortices. Furthermore, all the particles captured by a vortex asymptotically converge to a single point inside the vortex, and remain at rest there indefinitely. As B increases, the other four parameters remaining fixed, fewer and fewer particles are captured by the vortices. Finally, when B reaches the threshold value given by the solid curve (*a*), which is about 6.5 for $A = 5.0$, further increase in its value results in the disappearance of particle entrapment. Note that this threshold value corresponds to the bifurcation point in figure 11, and the disappearance of particle entrapment is due to the non-existence of the equilibrium points. On the other hand, the disappearance of the asymptotic convergence of particles to fixed points when we go from buoyant to heavy particles is due to the loss of stability of the equilibrium points (see figure 13). To further investigate the effects of the parametric inputs, we increase the free-stream Reynolds number to 300.0 in case (*b*). This causes the increase of the threshold value of B for particle entrapment; apparently, the increase in Re results in a larger viscous drag so that it can counteract a greater value of B. When the density parameter, ε, is increased, the threshold value of B decreases, as can be seen by comparing cases (*b*) and (*c*). This is intuitively clear since a larger ε means a particle with a greater buoyancy and, thus, a greater chance of avoiding the captivity inside a vortex. In some sense, this is similar to the finding of Thomas *et al.* (1983). In their paper, it is reported that a more buoyant particle, compared to a heavier one, can come closer to a line vortex with a horizontal axis, and avoid being captured by the vortex. Moreover, the entrapment width of the line vortex increases with the vortex strength (Thomas *et al.* 1983, 1984). This point is also consistent with the present study, as can be seen by comparing cases (*c*) and (*d*). Here, the strength of the Stuart vortices increases with k, and an increase in the parameter k results in the increase of the threshold value of B for particle entrapment. Finally, we point out that entrapment diagrams similar to figure 16 are also obtainable for bubbles ($\varepsilon = 2.0$) using the correlation proposed by Oliver & Chung (1987) for the drag coefficient f_d (Tio *et al.* 1993*b*).

To test the predictions of the asymptotic model of §3 for buoyant particles, we release 51 × 51 particles uniformly over a square of sides equal to 2π and co-centred with a cat's eye, and follow the evolution of the particle cloud. The asterisks in figures 17(*a*), 17(*b*) and 17(*c*) denote the initial position of those particles which are captured by the vortices and end up at the equilibrium points. We observe from figure 17(*a*) that all particles initially released below the x-axis end up in captivity, and that some particles released above the cat's eyes are also finally trapped inside the vortices. With $B = 0.02 < \mathscr{F}_{cr}/2\pi \approx 0.080$, this agrees with the predictions of §3. In figure 17(*b*), the gravity parameter B is increased beyond $\mathscr{F}_{cr}/2\pi$. In agreement with the analysis of §3, it is seen that all particles initially released above the cat's eyes escape to $y = \infty$. Furthermore, some of the particles which enter a cat's eye from below are able to escape from it. When ε is increased, corresponding to lighter particles, the region of attraction (i.e. the region composed of the initial positions of particles which are eventually trapped by the vortices at their respective equilibirum points) inside a cat's eye shrinks, as is seen from the comparison of figures 17(*b*) and 17(*c*). This is similar to the observation of Thomas *et al.* (1983) that the entrapment width of a line vortex with a horizontal axis is shorter for lighter buoyant particles. While the shrinking of the region of attraction inside a cat's eye in reponse to an increase in ε is intuitively clear, it is interesting to examine it from the point of view of §3. Observe from figures 10(*a*) and 10(*b*) that for a particle initially inside a cat's

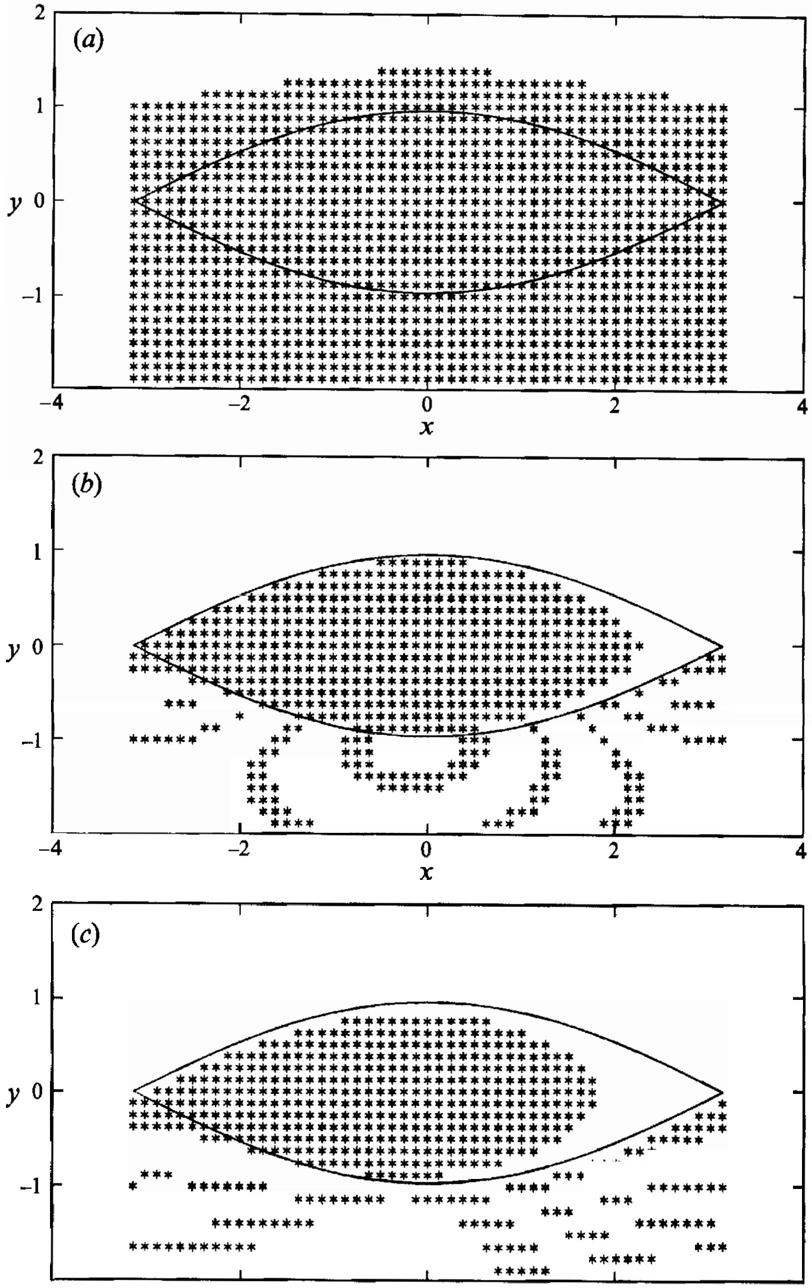

eye and close to its right-hand tip to remain trapped, it must be sufficiently close to the vortex centre so that its initial 'particle path function' satisfies the inequality

$$\Phi_{init} < \Psi_{cr} + \gamma\left(\tfrac{3}{2}\varepsilon - 1\right)\left(\mathscr{F}_{cr} - 2\pi B\right). \qquad (5.1)$$

Since $\mathscr{F}_{cr} - 2\pi B < 0$, an increase in ε results in a decrease of Φ_{init}, i.e. the shrinking of the region of attraction.

6. Concluding remarks

In this paper, we study the dynamics of heavy and buoyant particles in a periodic Stuart vortex flow. Based on the assumption of dominant viscous drag forces, we develop an asymptotic model so that we can study some aspects of particle motion analytically. In particular, it is shown that heavy and buoyant particles can be suspended against gravity in the flow, but by completely different mechanisms. For buoyant particles, suspension takes place at the stable equilibrium points, where particles spiral into and then remain at rest. On the other hand, heavy particles are suspended in motion along a single open periodic trajectory located above the cat's eyes. We point out here that heavy particles may also be suspended along quasi-periodic and chaotic trajectories located above and below the vortices, and that suspension of particles slightly heavier than the fluid in closed orbits is also possible (Tio *et al.* 1993*a*). However, these suspension modes of heavy particles require that the other forces acting on the particles are not diminishingly small compared to the viscous drag.

To test the validity of the asymptotic model, we first study the equilibrium points of the dynamical system (2.10)–(2.13). We find that when the equilibrium points exist, they are always unstable for heavy particles but there is one which is always stable for buoyant particles. This finding is consistent with the two different suspension mechanisms for buoyant and heavy particles predicted by the asymptotic model. For further tests of the asymptotic model, we then carry out a computational study by integrating numerically the equations of motion of the particles. Generally, the computational results are in agreement with the analytical predictions based on the assumption of dominant viscous drag.

In some cases, the Stuart vortex flow can be used as a model for the plane free shear layer. In fact, it has been numerically found to be a final equilibrium state of the two-dimensional shear layer under some restrictive conditions (Sommeria, Staquet & Robert 1991). Nevertheless, the Stuart vortices are, in general, only a crude representation of the vortical structures observed in the shear layer. Usually, these structures evolve in time and space, and interact with each other. Their evolution and interaction will certainly alter the structure of the asymptotic trajectory predicted in §3 for heavy particles. However, the entrapment of buoyant particles in the central region of the vortices will persist since the underlying mechanism is, basically, local to the individual vortices.

The authors wish to thank the United Technologies Corporation for a gift supporting the research reported here. The partial support by the United States Office of Naval Research (Grant No. N00014-91-J-1252) is also acknowledged.

REFERENCES

Auton, T. R., Hunt, J. C. R. & Prud'homme, M. 1988 The force exerted on a body in inviscid unsteady non-uniform rotational flow. *J. Fluid Mech.* **197**, 241–257.

Chein, R. & Chung, J. N. 1987 Effects of vortex pairing on particle dispersion in turbulent shear flows *Intl J. Multiphase Flow* **13**, 785–802.

Chein, R. & Chung, J. N. 1988 Simulation of particle dispersion in a two-dimensional mixing layer. *AIChE J.* **34**, 946–954.

CHUNG, J. N. & TROUTT, T. R. 1988 Simulation of particle dispersion in an axisymmetric jet. *J. Fluid Mech.* **186**, 199–222.

CLIFT, R., GRACE, J. R. & WEBER, M. E. 1978 *Bubbles, Drops, and Particles.* Academic.

CRISANTI, A., FALCIONI, M., PROVENZALE, A. & VULPIANI, A. 1990 Passive advection of particles denser than the surrounding fluid. *Phys. Lett.* A **150**, 79–84.

CROWE, C. T., GORE, R. A. & TROUTT, T. R. 1985 Particle dispersion by coherent structures in free shear flows. *Particulate Sci. Technol.* **3**, 149–158.

DANDY, D. S. & DWYER, H. A. 1990 A sphere in shear flow at finite Reynolds number: effect of shear on particle lift, drag, and heat transfer. *J. Fluid Mech.* **216**, 381–410.

GAÑÁN-CALVO, A. M. & LASHERAS, J. C. 1991 The dynamics and mixing of small spherical particles in a plane, free shear layer. *Phys. Fluids* A **3**, 1207–1217.

MANTON, M. J. 1974 On the motion of a small particle in the atmosphere. *Boundary-Layer Met.* **6**, 487-504.

MAXEY, M. R. 1987 The motion of small spherical particles in a cellular flow field. *Phys. Fluids* **30**, 1915–1928.

MAXEY, M. R. & RILEY, J. J. 1983 Equation of motion for a small rigid sphere in a nonuniform flow. *Phys. Fluids* **26**, 883–889.

MCLAUGHLIN, J. B. 1991 Inertial migration of a small sphere in linear shear flows. *J. Fluid Mech.* **224**, 261–274.

MEI, R. 1992 An approximate expression for the shear lift force on a spherical particle at finite Reynolds number. *Intl J. Multiphase Flow* **18**, 145–147.

MEI, R., LAWRENCE, C. J. & ADRIAN, R. J. 1991 Unsteady drag on a sphere at finite Reynolds number with small fluctuations in the free-stream velocity. *J. Fluid Mech.* **233**, 613–631.

NIELSEN, P. 1984 On the motion of suspended sand particles. *J. Geophys. Res.* **89**, 616-626.

OLIVER, D. L. R. & CHUNG, J. N. 1987 Flow about a fluid sphere at low to moderate Reynolds numbers. *J. Fluid Mech.* **177**, 1–18.

REEKS, M. W. & MCKEE, S. 1984 The dispersive effects of Basset history forces on particle motion in a turbulent flow. *Phys. Fluids* **27**, 1573–1582.

SAFFMAN, P. G. 1965 The lift on a small sphere in a slow flow. *J. Fluid Mech.* **22**, 385–400. Also Corrigendum, **31**(1968), 624.

SIMON, B. & POMEAU, Y. 1991 Free and guided convection in evaporating layers of aqueous solutions of sucrose. Transport and sedimentation of solid particles. *Phys. Fluids* A **3**, 380–384.

SOMMERIA, J., STAQUET, C. & ROBERT, R. 1991 Final equilibrium state of a two-dimensional shear layer. *J. Fluid Mech.* **233**, 661–689.

STOMMEL, H. 1949 Trajectories of small bodies sinking slowly through convection cells. *J. Marine Res.* **8**, 24–29.

STUART, J. T. 1967 On finite amplitude oscillations in laminar mixing layers. *J. Fluid Mech.* **29**, 417–440.

THOMAS, N. H., AUTON, T. R., SENE, K. & HUNT, J. C. R. 1983 Entrapment and transport of bubbles by transient large eddies in multiphase turbulent shear flows. In *Physical Modelling of Multiphase Flow*, pp. 169–184. BHRA Fluid Engineering.

THOMAS, N. H., AUTON, T. R., SENE, K. & HUNT, J. C. R. 1984 Entrapment and transport of bubbles by plunging water. In *Gas Transfer at Water Surfaces* (ed. W. Brutsaert & G.H. Jirka), pp. 255–268. D. Reidel.

TIO, K.-K., GAÑÁN-CALVO, A. M. & LASHERAS, J. C. 1993*a* The dynamics of small, heavy, rigid spherical particles in a periodic Stuart vortex flow. *Phys. Fluids* A **5**, 1679–1693.

TIO, K.-K., LASHERAS, J. C., GAÑÁN-CALVO, A. M. & LIÑÁN, A. 1993*b* The dynamics of bubbles in periodic vortex flows. *Appl. Sci. Res.* (in press).